May 2019

Dynamic change of Cardiomyocytes on Shape Memory Polymer

Shiyang Sun
Syracuse University

Abstract

In the previous work, it has been proven that substrate topography can influent the cell behaviors, including morphology and functions. Many research teams showed that wrinkled surfaces have been able to improve the alignment and orientation of different biological cell types. Cardiomyocytes are also influenced by the surface topography with better alignment along the winkles, comparing to the flat surface. However, there is little evidence to demonstrate how cardiomyocytes would respond to the wrinkle formation and achieve the cellular alignment change during the transition from flat surface to topographic surface. In this thesis, we have created a dynamic substrate based on shape memory polymer to change the surface topography and induce the nanoscale wrinkle formation. Using this dynamic substrate, we can observe the cardiomyocyte responses to topography changes, and investigate the dynamic reorganization progress of myofibril remodeling during the cell alignment.

Key words: cardiomyocyte, alignment, shape memory polymer, surface topography

Dynamic change of Cardiomyocytes on Shape Memory Polymer

By

Shiyang Sun

B.S. Biological Pharmacy, Jilin University, China, 2013

Thesis

Submitted in partial fulfillment of the requirements for the degree of

Master of Sciences (M.S.) in *Bioengineering*

Syracuse University

May 2019

Table of content

List of Figure

List of Table

1. Introduction

1.1. Cardiomyocyte Structure and Organization

1.1.1. Introduction of Cardiomyocyte

Three types of muscle exist in body: skeletal muscle, smooth muscle and cardiac muscle. The muscle cells contain sarcomeres, which are the basic structural and functional unit for muscle contraction. A series of sarcomeres constitute the myofibril, which then constitute fascicles. The fascicles form the muscle fibers, and fibers constitute the entire muscle (**Figure 1**). Unlike the other two muscle types, cardiac muscle can only be found in the heart. Cardiac muscle has a similar structure to skeletal muscle. Compared to skeletal muscle cells, cardiac muscle is not linear and often have branches. Moreover, T-tubules are larger but less in cardiomyocytes than in skeletal muscle, which restore more calcium ion. In addition, the intercalated disc is a unique structure, which can only be found in the cardiac muscle and provides strong mechanical linkage between cardiomyocytes. Through this structure, action potential can spread to the whole cardiac muscle with high speed in low resistance[1].

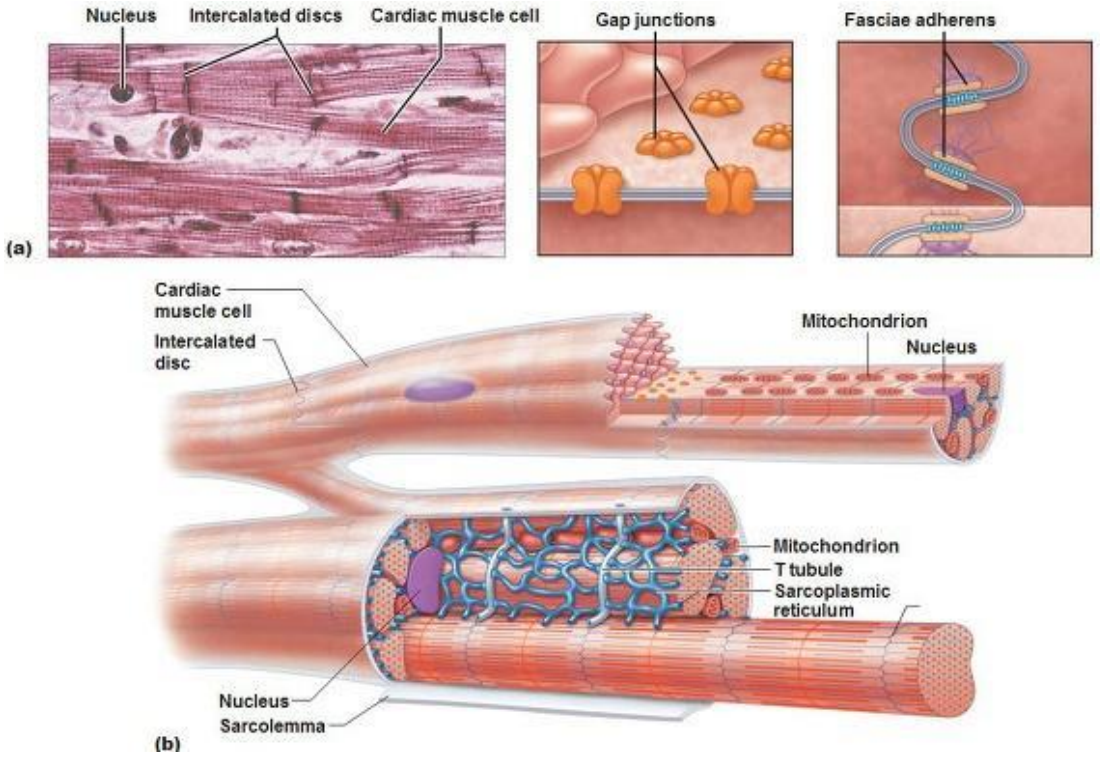

Figure 1 The unique structures of heart muscle[2].

1.1.2. Sarcomere Structure and Myofibril Organization

Cardiomyocytes are the main cellular component of cardiac muscle. In the mature cardiomyocytes, about 50 sarcomeres make up the myofibrils; whereas, approximately 50 to 100 myofibrils constitute one cardiomyocyte[3]. Cardiomyocytes are cylinder-shaped with an average length of about 100 μm and an average diameter of about 10 μm[4]. The cardiomyocytes persistently beat over 3 billion times in the whole human lifespan[5].

The sarcomere is the fundamental repeating contractile unit within the myocytes[1,6], including the structure between two z-lines, which consist of actinin (**Figure 2**). The sarcomeres are mainly composed of two transverse filament systems, which are the thick filaments and thin

filaments[6]. The resting length of sarcomere is about 1.8 to 2.4 μm and can shorten to about 70% of the original length[6–8]. Sarcomeres are constituted by multiple proteins, including myosin, actin, titin, tropomyosin, and the troponin complex. Myosin and actin are the main elements of sarcomeres; whereas, other proteins function in complimentary roles[6,7]. The main protein component of thin filament is actin, and the main protein component of thick filament is myosin. One end of thin filaments connects to the z-disk, and the other end organizes towards the center of sarcomeres. On the contrary, the thick filaments do not connect to the z-lines, they are located in the center of the sarcomeres with one end connecting to the M line. The thin filaments and thick filaments are consistently interacting through the cross-bridge, which is formed by the golf club shape head of myosin molecules. Through conformational change of the cross-bridge, thin and thick filaments increase overlap and produce the contraction.

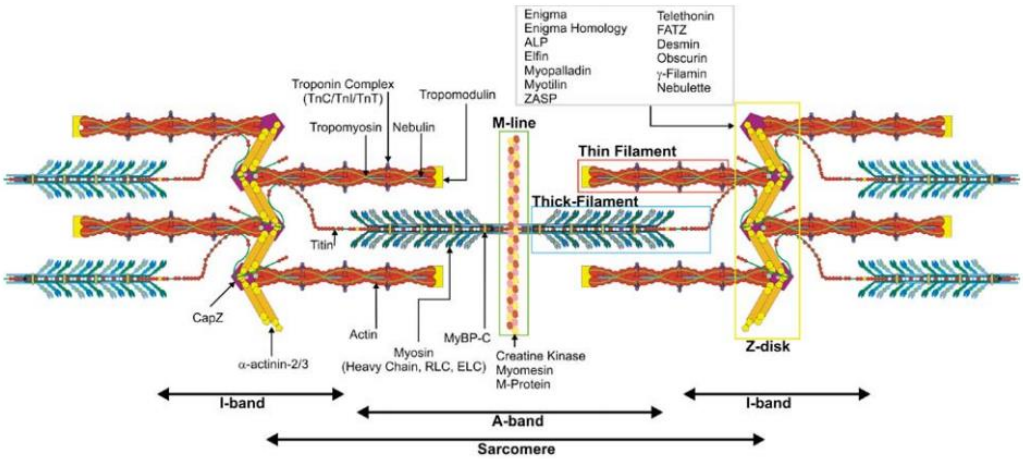

Figure 2 Molecular structure of sarcomere. The main elements of sarcomere are thin filaments and thick filaments, which are respectively consisted by actin and myosin[8].

Myofibrils consist of repeating sarcomeres and align along with the muscle fiber direction and extend to the entire muscle fiber. From the cross section, it shows that each thick filament is surrounded by 6 thin filaments, and each thin filament is surrounded by thin filaments and 3

thick filaments (**Figure 3**). The diameter of myofibril is about 1~2 μm. It has been proposed that the myofibrillogenesis is related to the onset of rhythmic contractions[9]. At the beginning of myofibrillogenesis, the concentration of sarcomere proteins increases in the cytoplasm. Within several hours, titin dots appear on the plasma membrane, which provide the binding sites of α-actinin and form nascent Z bodies, the precursor of Z-disc. Actin assembles near the cell membrane and constitutes I–Z–I complexes based on the Z bodies. Several hours later, M-line appears in the cytoplasm, and titin protein helps thick filament formation. Moreover, during the formation of thick filament, myomesin might play an important role to anchor the myosin filament with titin filament, similar to the function of α-actinin to anchor the actin filament with Z-disc[10]. Finally, myosin filaments associate with actin filaments to form new sarcomeres, and sarcomeres compose myofibrils which extend to the entire cardiomyocyte[11].

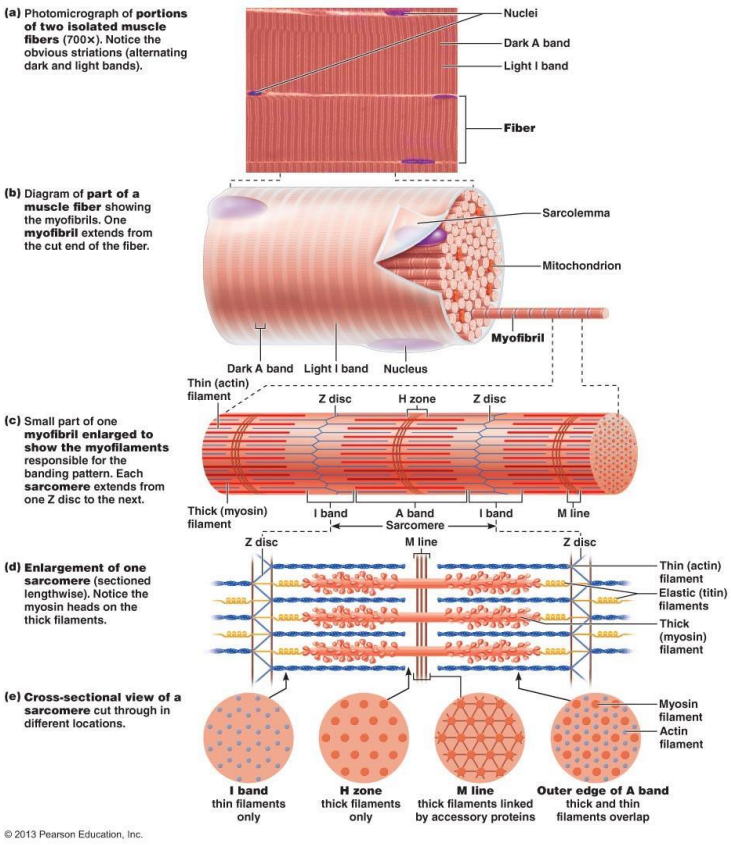

Figure 3 The multiscale myofibril architecture and muscle fiber structure[2].

1.1.3. Cell Adhesion

Cell adhesion is involved in mechanical signaling, cell migration, cell differentiation, and cell survival[12]. The change of cell adhesion can induce pathological change[13], including arthritis[14], cancer[13,15], osteoporosis[16], and atherosclerosis[17]. Most mammalian cells are anchorage-dependent and attach to the underneath substrates by anchoring to the extracellular matrix (ECM)[18]. Cell adhesion regions demonstrate more chemical bonds between cell membrane proteins and ECM components. Cell adhesion is achieved by the interactions among multiple protein complexes that are primarily consisted by three protein categories, including cell adhesion molecules, ECM proteins, and cytoplasmic plaque/peripheral membrane proteins.

The cell adhesion receptors are usually transmembrane glycoprotein, such as integrins, cadherins, immunoglobulins, selectin, and proteoglycan superfamilies[19]. ECM proteins are usually large glycoprotein molecules or clusters, such as collagens, fibronectins, laminins, and proteoglycans. On the intracellular side of cell membrane, peripheral membrane proteins, such as vinculin, talin and catenin, connect the adhesion receptors to the cytoskeletons (**Figure 4**)[20–23] to form a stable attachment between cell and the ECM.

For cardiomyocytes, costameres are used to describe the vinculin-containing, rib-like band perisarcolemmal subcellular structure, which is perpendicular to its long axis[24,25] and align predominantly with Z disks[26] (**Figure 4**). Costameres have three major functions: to keep plasma membrane, or sarcolemma, aligned with nearby sarcomere; to protect sarcolemma damage from cell contraction; or to transmit some contraction force from cell to ECM[27]. Similar to the other cell type, vinculin is the marker protein of this structure[26]. Costameres connect with the Z-line and overlie the I-band of cardiomyocytes[28]. Costameres also connect with ECM protein via integrins and to neighboring cardiomyocyte. In recent year, costameres are assumed to play an important role as a lateral mechanical sensor of cardiomyocytes with two distinct macromolecules complex, including integrin complex and the dystrophin-glycoprotein complex[28,29]. Integrins are essential components for communication between cardiomyocyte cytoskeleton and ECM[30]. Dystrophin glycoprotein complex (DGC) is special protein complex in skeletal muscle cells and cardiomyocytes, and DGC has the function as signaling and stabilizing mechanism of interaction between cytoskeleton, membrane, and extracellular matrix[31].

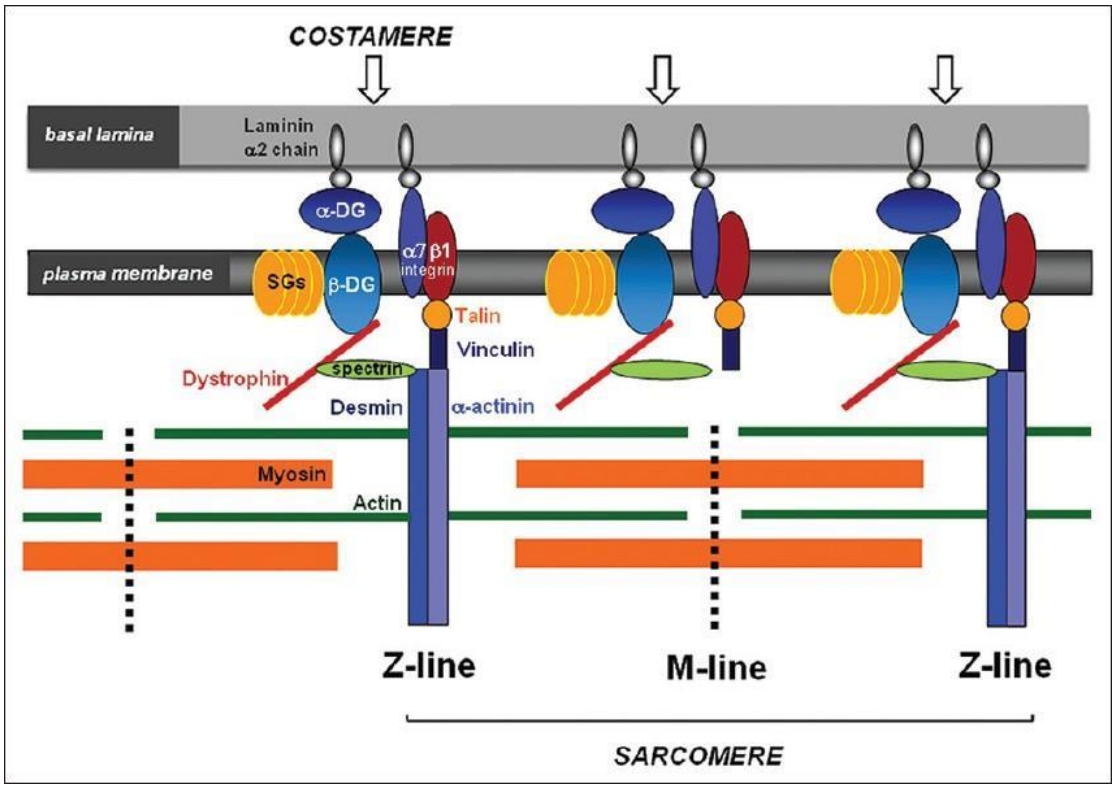

Figure 4 Costamere is the key structure to link sarcomere and ECM. Costamere shows rib-like pattern and lies at the sarcolemma over the Z and M lines. Integrin complex and DGC plays important roles in connection between sarcomeres and ECM[32].

Cardiomyocytes form a dense focal adhesion with vinculin and other cell skeletal protein and connects to ECM[33]. Vinculin is a membrane-associated protein which links the actin to the sarcolemma. Vinculin directly connects integrin with the associated protein talin and actinin and can be found at cell-cell and cell-ECM binding sites[34] (**Figure 5**). Thus, the ECM-integrin-costameric protein network consists of the cardiomyocyte adhesion model, and cardiomyocytes transduce the beats to ECM within this model.

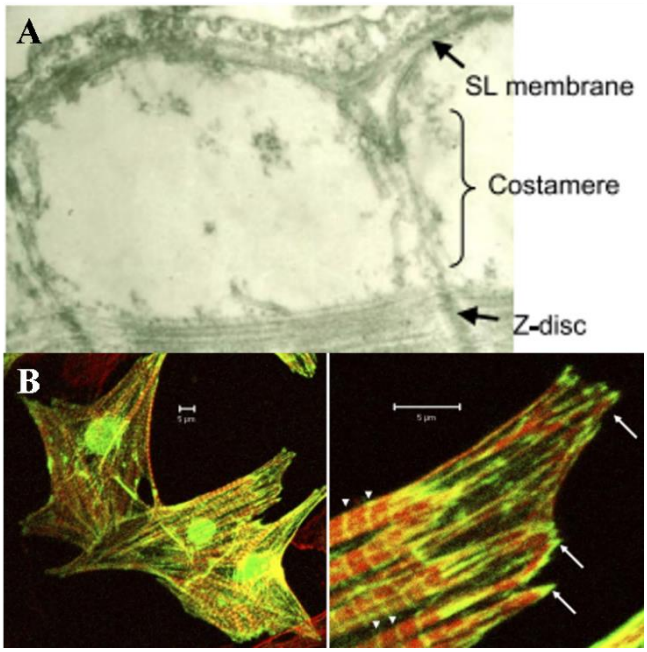

Figure 5 Focal adhesion model of cardiomyocytes. (A) Cardiomyocytes attach the ECM through costameres, and it shows that costameres play very important role to connect contractile units (Z-disc) with membrane. (B) It shows the costamere structure with fluorescence. Cells were stained with focal adhesion kinase (FAK), focal adhesion-related nonkinase (FRNK, green) and actin (red) and noted the costameric (arrowhead) and focal adhesion (arrow) in right image. All scale bar is 5 μm[28].

1.1.4 Cell Alignment Regulate sarcomere

Extracellular matrix (ECM) has been proved to be important to morphological maintenance of cells. Cardiomyocytes receive mechanical signals from outer ECM through transmembrane receptor, such as integrin[35]. Cells are able to receive and utilizing extracellular mechanical signal with focal adhesion complex (FAC) to assemble actin filament and grow[28]. Cells recruit the FAC into adhesion region, and high stress is transmitted into cells, which triggers the polymerization of actin filament from focal adhesions[36]. Furthermore, mechanical signals and force can be transduced to biochemical signals to trigger the change of filament protein synthesis and polymerization and gene expression inside the cells[37].

The impact of ECM on cell morphology change has been improved for decades[38]. In recent years, new technologies and designs allow researchers to study the impact of ECM to single cell with mechanical stimulation, and results show cell will response to mechanical stretch[39]. Parker et al. shows that ECM and cell shape are an important signaling for myofibrillogenesis and sarcomere direction, and with increasing aspect ratio of cells, most myofibrils are restricted to parallel to long cell axis, which is also cells alignment direction (**Figure 6**)[35].

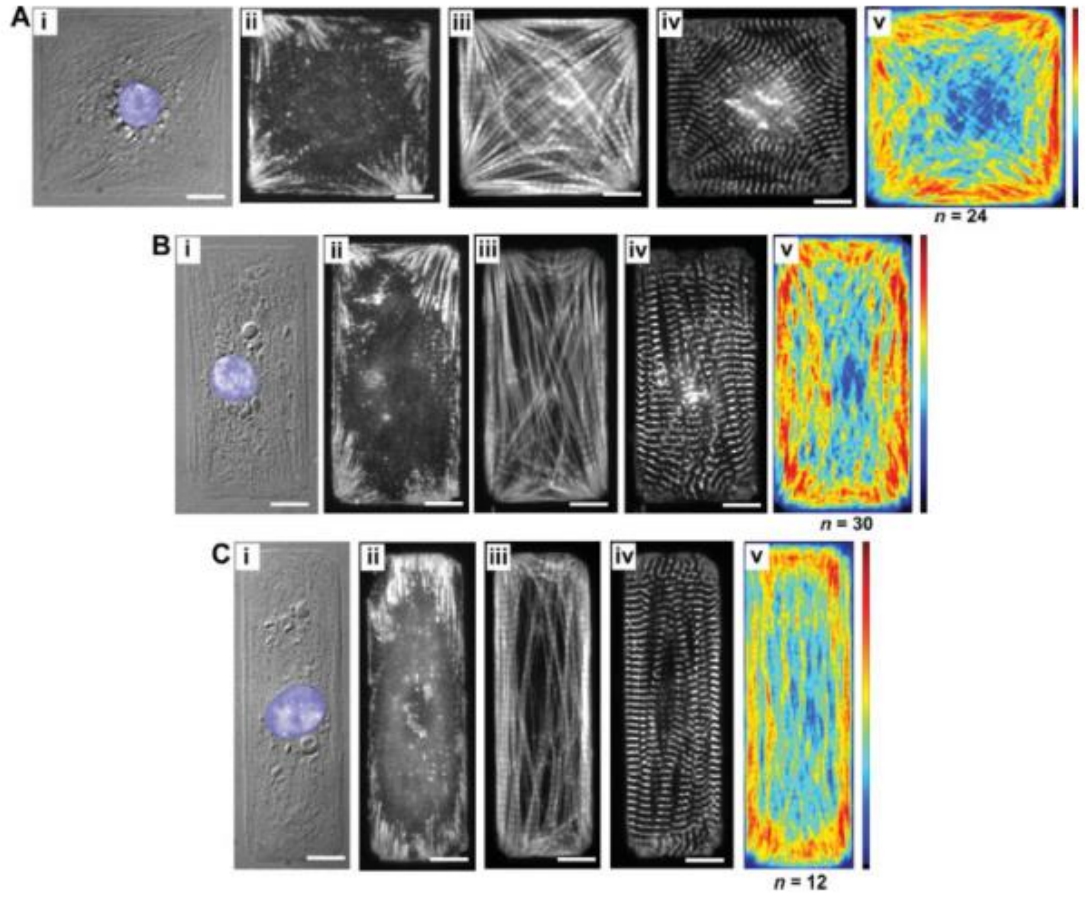

Figure 6 Effect of cell alignment on sarcomere direction. As aspect ratio of cell increase, the direction of myofibril is restricted to parallel to long cell axis, and aspect ratio of cell is 1:1 (A), 2:1 (B) and 3:1 (C)[35].

1.2. Surface Topography and Cardiomyocyte Alignment

1.2.1. Topography Control Myofibril Organization

ECM proteins show abundant nanometer-scale structure and contribute cell-matrix interaction. The basement membranes of tissues exhibit nanotopography and interact with neighboring cells[40,41], and individual ECM molecules also show the nanotopographic features, such as collagen[42]. Contact guidance is the major response of cells to micron or nanometer scale topographical structure, and it is an essential component to regulate multiple cell function and behavior, such as migration and morphology[43].

In recent years, the development of micro and nanofabrication technology has enabled researchers to design and fabricate substrate that allow the native scale topography and structure to appear on two-dimensional substrate[44]. The substrate surface topography has been used to control the cell adhesion, orientation, movement, proliferation and differentiation[45–47]. The ordered topographic patterns and structures are normally in the scale of submicron or even smaller. Cells can detect the surface features, respond to the mechanical signals, and change their morphology and gene expression[48]. It has been shown that the interactions between cells and ECM have important functions in various biological mechanism, including angiogenesis[49], embryogenesis[50], and tumorigenesis[51].

For a better understanding of cell-ECM interactions, different surface designs have been used in many research areas, including nanofibers, nanogratings, nanopillars and nanopits[52], to regulate the behavior of the cells[53]. S. R. Bhattarai et al. selected PEG, PLA and PDO as the

material, and through electrospinning, the copolymer PPDO/PLLA-b-PEG has been fabricated as nonwoven, three-dimensional, porous, and nanoscale fiber-based matrix. The result showed the nanofiber structure hugely increased the surface area of structure, which promoted cell proliferation and allowed cells to migrate across fibers (**Figure 6**)[54]. Christopher J. Bettinger et al. showed that multiple cell types exhibited responses to nanogratings, including fibroblasts, endothelial cells, stem cells, smooth muscle cells, epithelial cells, and Schwann cells. It was observed that nanograting improved cell alignment and elongation parallel nanograting axis according to the increasing of depth[44] (**Figure 7**). Md. Abdul Kafi et al showed stronger adhesion and larger spreading of cell on nanopillars structure in their research. Compared to 2D designs, 3D nanopillars promoted cell adhesion by increasing cell binding sites with integrin receptor, which increased the links with substrate but decreased cell migration[55] (**Figure 8**). In other research, nanopits structure design was proved to decrease cell adhesion and spreading due to the change of physical force[52,56] (**Figure 9**).

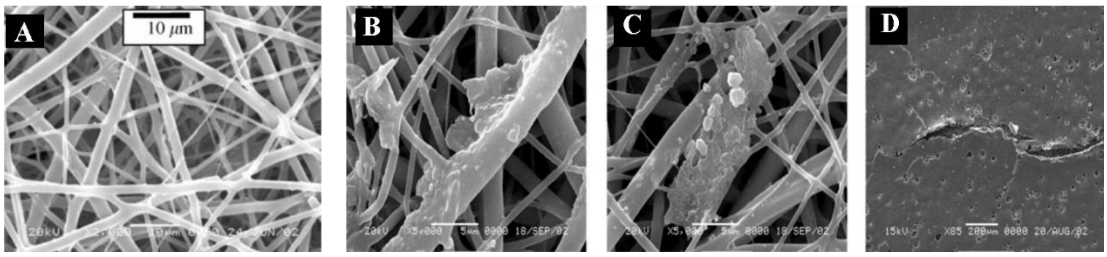

Figure 7 SEM images of nanofiber. (A) Morphology of nanofiber structure, which is fabricated by electrospinning. (B)(C)(D) Nanofibers are suitable for cell proliferation. The right image shows different time points of NIH 3T3 cell growth, including after 3 days (B), after 5 days (C) and after 10 days (D)[54].

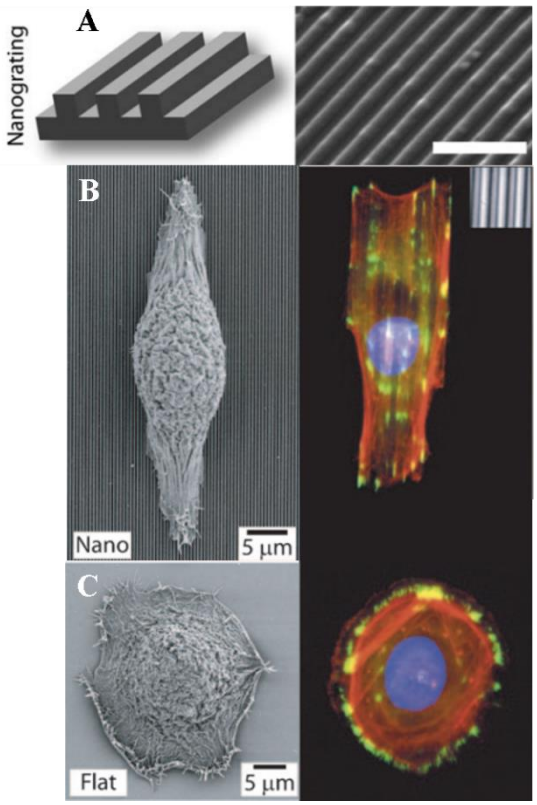

Figure 8 Nanograting design. (A) Design of nanograting, and right image is SEM of nanograting. (B)(C) Comparison between cell seeding on nanograting and flat surface. On the nanograting surface (B), the cell shows better alignment than flat surface (C)[44].

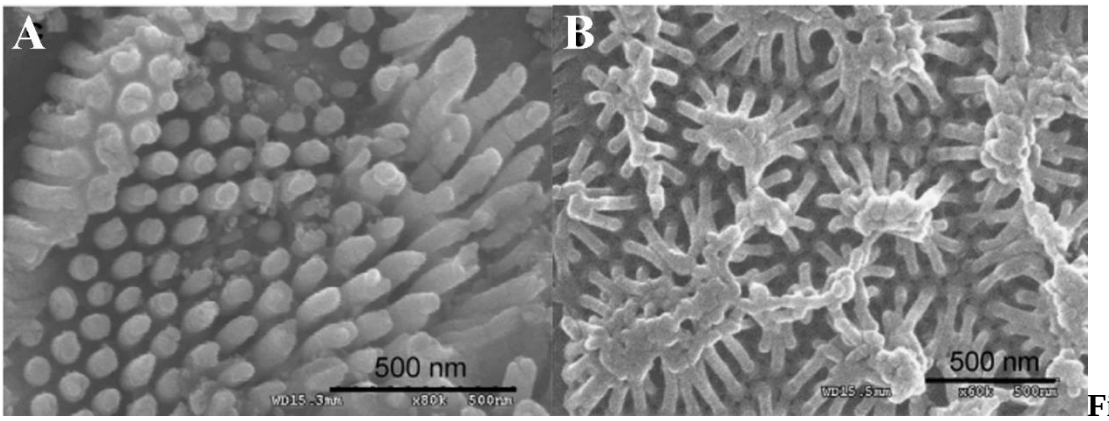

Figure 9 SEM images of nanopillars. (A) SEM of nanopillars. (B) Nanopillars with cells. Scale bar is 500 nm[55].

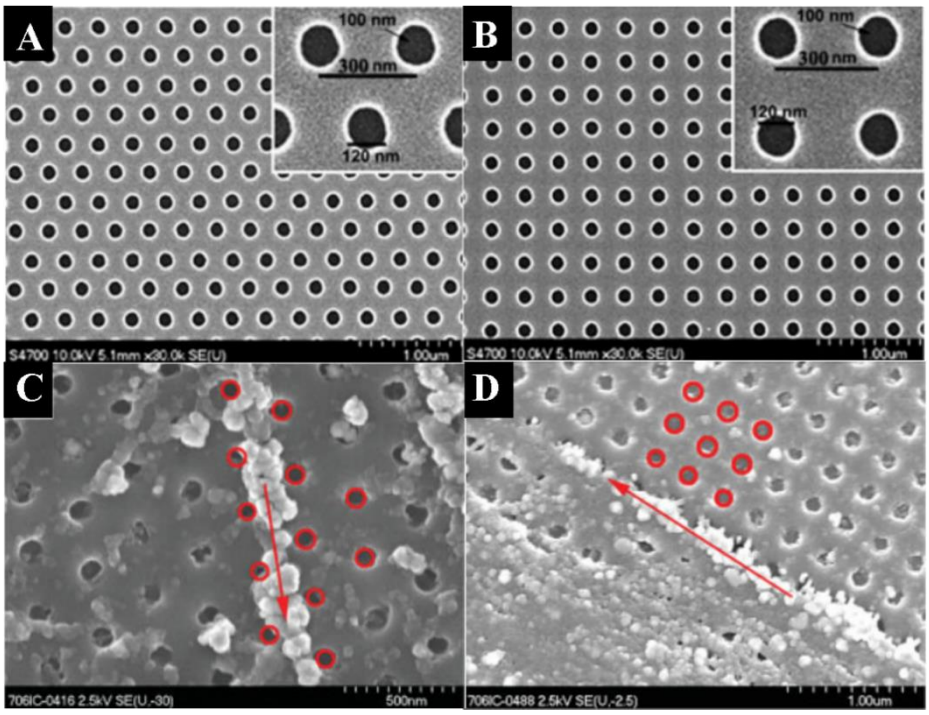

Figure 10 SEM images of different nanopits design. (A)(B) Same size of nanopits but different array, including hexagonal nanopit array (A) and square nanopit array (B). (C)(D) Although the designs are different, both of them decreased the cell adhesion[57].

Surface buckling and surface wrinkles are two common natural phenomena to create patterned surface topography[58]. Several methods have been used to generate wrinkled surface, including thermal contraction[59], external compressive force[60], and differential swelling or shrinkage[61]. It has been shown that surface topography affects the alignment and anisotropic elongation of cultured cardiomyocytes.

Au et al. selected Polyvinyl carbonate as the materials of substrate to respectively discuss and compare the effects of topography and electricity current to cells. Researchers abraded surface of substrate to create topography on surface and placed samples between two carbon electrodes to create electricity current. According to the results, surface topography and electricity current both affected cells morphology, and cells showed better alignment and higher elongation

parallel to the direction of topography and electricity current. However, compared with electricity current, surface topography showed stronger effects on cells, which was shown by smaller angle and larger aspect ratio of cardiomyocyte alignment[62] (**Figure 10**).

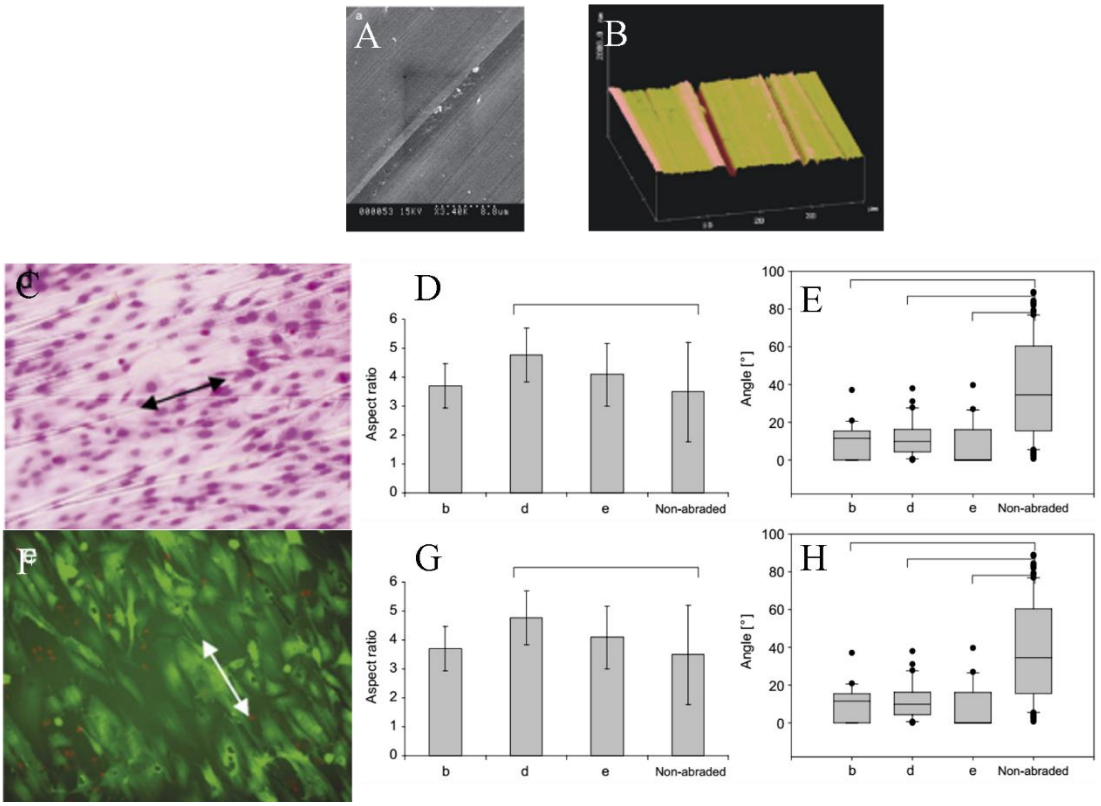

Figure 11 Results from Au's work. (A) SEM image of Polyvinyl carbonate substrate with abrasive surface. (B) AFM image of the substrate surface. (C-E) Results of fibroblast growth on the abrasive surface. Topography improved the aspect ratio (D) but decreased the cell orientation angle (E). (F-H) Results of cardiomyocyte growth on the abrasive surface. Topography improved the aspect ratio (G) but decreased the cell orientation angle (H)[62].

Moreover, Kim et al. chose to use polyethylene glycol (PEG) hydrogel as materials to make anisotropically nanofabricated substratum (ANFS), which has ordered ridges and grooves. After several days cardiomyocytes culture, result has proved topography will influence cardiomyocyte's behavior, such as morphology and action potential. After 48 hours culture, cells showed higher length and lower width than unpatterned samples, and length increases as

culture time is increased. In addition, cell orientation results showed that topography affected cardiomyocytes alignment direction to parallel ridge/groove direction[63] (**Figure 11**).

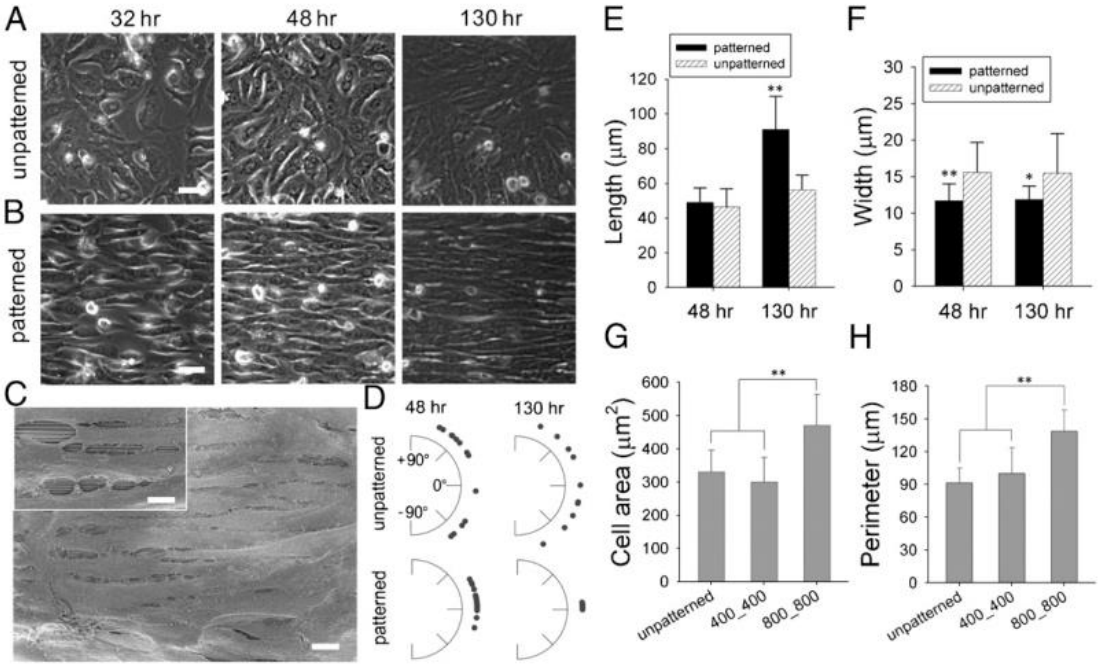

Figure 12 Cell reorientation on patterned surface. (A)(B) Cardiomyocytes shows clear alignment trend on topographical surface, but not on the unpattern surface. (C) SEM images of cells on the patterned surface. (D) Surface topography affects the cells to align parallel to ridge/groove direction. (E)(F) Quantification results of cell length and width. On the patterned surface, cells have higher length and lower width. (G)(H) Pattern also increases the area and perimeter of cells[63].

McDevitt 's team in 2003 used the method of Skarja and Woodhouse[12] to synthesize Polyurethane (PU) substrate and improve their design with surface modification. PU substrate was modified with PU solvent cast and sterilized by UV light to create surface topography. Then, McDevitt's team selected rat's cardiomyocyte to seed on the surface to test the effect of topography to cardiomyocyte with comparison with cell seeding on glass cover slip. From their results, it showed that McDevitt's team used their method to successfully create surface, and topography and pattern showed strong effects to cardiomyocytes alignment[64] (**Figure 12**).

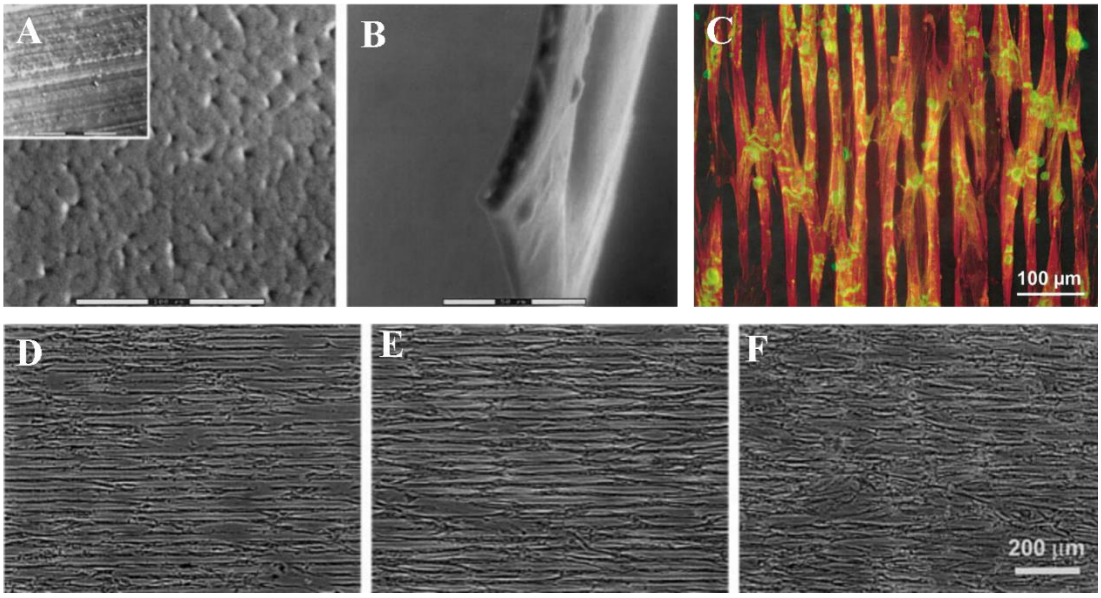

Figure 13 Effect of PU patterning on cardiomyocyte alignment. (A)(B) SEM images of advanced design of PU from McDevitt's team with surface topography, including transverse SEM (A) and cross-section SEM (B). (C) Rat neonatal cardiomyocytes were seeded on PU surface with topography, and cardiomyocyte showed good alignment. (D)(E)(F) Different time points of cardiomyocytes on PU surface, including day 2 (D), day 6 (E) and day 10 (F). Scale bar is 200 μm[64].

In 2014, Luna's team studied the effect of multiple scale topography to embryonic stem cells derived cardiomyocytes. Luna's team used metal with topography as a mold to create other material substrates with surface topography following method from Fu's team[65]. Luna's team chose to use polystyrene (PS) sheets as baseboard and prestress sheets to create wrinkle on surface, and then, with different thickness gold sputter coating to create different metal wrinkle (**Figure 13**). Then, PS sheet with gold wrinkle was treated as mold to create PDMS substrate with surface wrinkle. The cell resource was selected from neonatal mice and euthanized after birth, and cells were treated with trypsin and seeded on PDMS substrate. Fibroblasts were also extracted and purified as control cells. Finally, the result showed that comparing to the flat surface, both cardiomyocytes and hESC-CMs had better alignment. In the nuclei analysis, it also showed that CMs had better alignment than the control group, and surface topography

improved the alignment of CMs and hESC-CMs[66] (**Figure 14**).

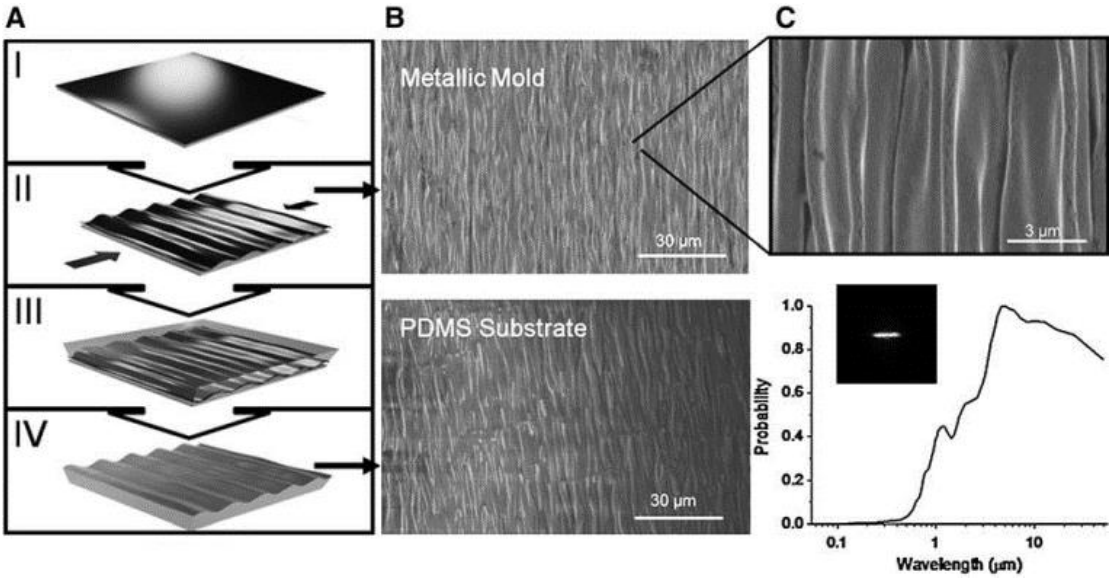

Figure 14 (A) Process of PDMS substrate fabrication with surface topography. (B) SEM images of metallic mold with wrinkles and PDMS substrate with wrinkles. (C) Zoom in image of the mold[66].

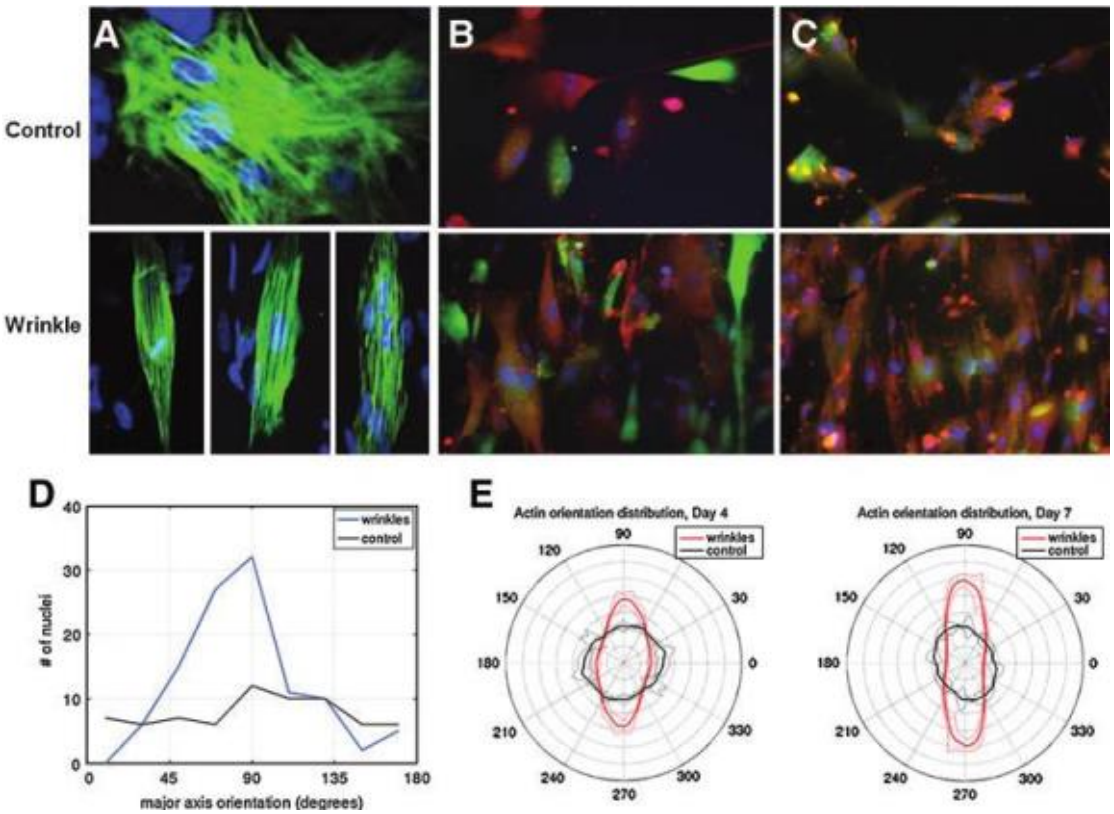

Figure 15 Results of hESC-CMs cultured on the PDMS substrate with wrinkles. (A)

Fluorescence staining of hESC-CMs with tropomyosin (green) and nuclei (blue). (B)(C) MLC2v-GFP cell line of hESC-CMs (green) with actin staining on surface at Day 4 (B) and Day 7 (C). (D)(E) Quantification result of hESC-CMs alignment, orientation[66].

In 2011, Wang's team selected Polyurethane (PU) and polystyrene (PS) as substrate materials. PDMS was used to make a wafer by using electron beam lithography and dry etching. PDMS wafer was designed as 450 nm in groove/ridge width and two different depth (100nm and 350nm), and PU and PS was covered by PDMS wafer to create two different substrates with different surface topography. The cells were harvested from the neonatal Wistar rats and seeded on PU and PS substrate in different density. Although different designs have different depth groove, both surface topography shows effect to cardiomyocytes alignment, including small angle and higher elongation, and deeper groove has larger effect to cardiomyocytes. In addition, cardiomyocytes have more beats on substrate with deeper groove. The topography of surface will generate more stress to the cells. The orientation and elongation of cardiomyocytes was mainly affected by the nanotopography groove depth, because of increasing formation of actin and focal contacts[67] (**Figure 15**).

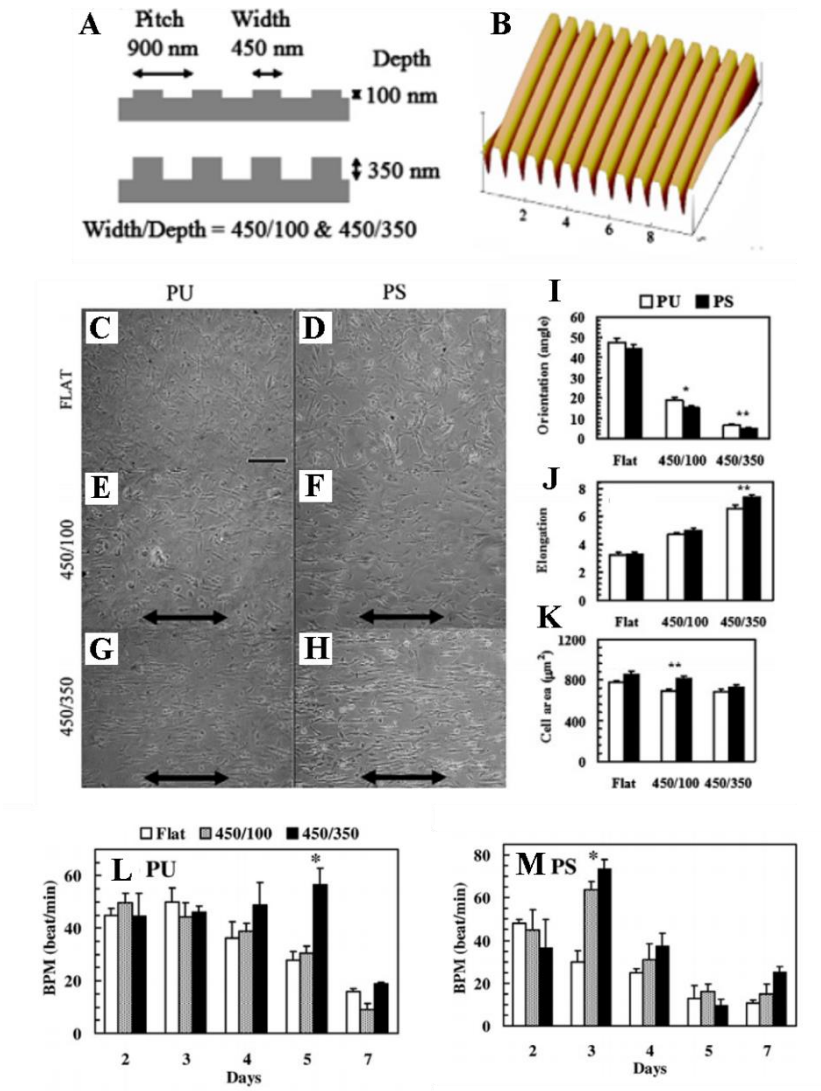

Figure 16 Wang team's design of ridge/groove topography. (A) Design schematics. (B) AFM image of 450/350 substrate. (C-H) Morphology of cardiomyocytes in culture for 2 days on different materials substrates with different surface topography design. (I-K) Quantification results of cardiomyocyte culture on different materials with different surface topography. (L)(M) Beating data of cardiomyocytes on different materials with different surface topography[67].

1.2.2. Shape Memory Polymer

Shape memory polymers (SMPs) have attracted significant attention from both industrial and academic researchers due to their useful and fascinating functionality[68]. The shape memory polymer is defined as the polymer which has the ability to memorize and recover to certain

shapes under certain situations. Different from shape memory alloy, shape memory polymers are able to transfer between two shape conditions though setting up a temporary intrinsic elastic polymeric network, which usually recovers under high temperature[68]. Shape memory polymers have both crystalline and amorphous structure, which allows them to transition between two different structures[69].

Thetert-Butyl Acrylate (TBA) monomer polymers are able to be used for shape storage[70]. TBA has very good thermal reducibility, reaching to 100% strain recover under high temperature[71]. Although the glass transition temperature of TBA is 65 °C, TBA polymers still are able to slowly recover at temperature below glass transition temperature. Because of the ability of shape recover, researchers use tBA as materials to fabricate substrate, and with shape recover, TBA polymer triggers surface coating shape change, form wrinkle and create target surface topography. In 2013, Yang's team used TBA and BA copolymer as material of substrate to produce SMP with crosslinker, TEGDMA (triethylene glycol dimethacrylate), and photoinitiator DMPA (2,2-dimethoxy-2-phenyl acetophenone). Copolymer solution with mold was placed in UV box to crosslink together, and resulting polymer was place in methanol for 6 hours for washing and vacuum oven under 55°C for overnight. Polymer was stretched at 80°C to different ratio length and sputter coated with gold to form a 33 nm thickness layer. Polymer with gold coating was place at 55°C for 30 minutes, and as polymer recover shape, it triggers wrinkle formation of gold layer. HASCs was seeded on polymer wrinkled surface to test wrinkle effect. Cells show different result on different polymer, and cell have clear alignment on wrinkle surface. For active surface cell culture, cells didn't show any order before

wrinkle formation, but cell change their alignment to same direction after wrinkle formation[58] (**Figure 16**).

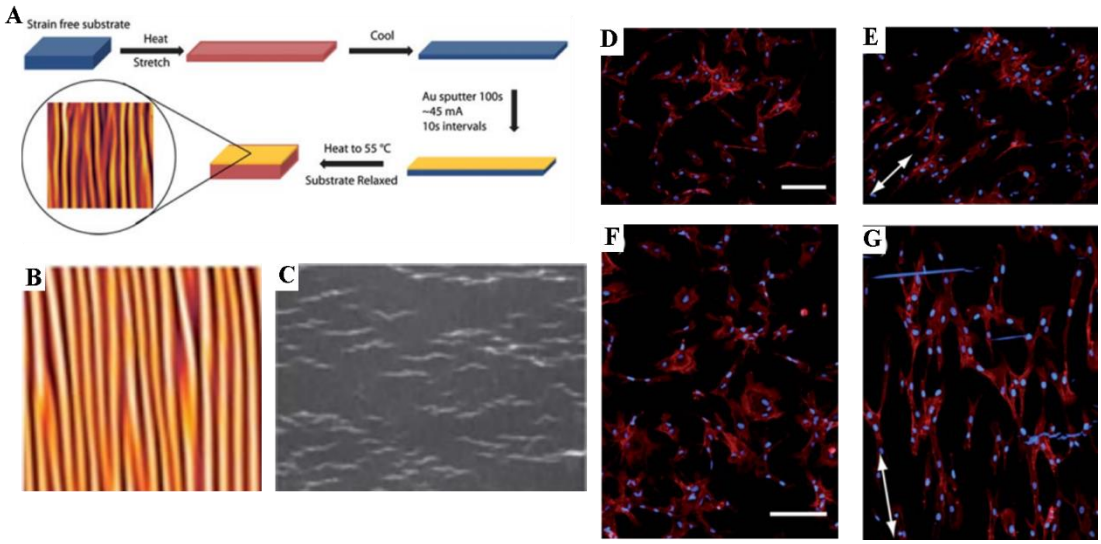

Figure 17 Shape memory polymer study. (A) Process of wrinkle formation on SMP. (B)(C) AFM and OM crack images of SMP substrate with wrinkle. (D)(E) Cells seeded on flat surface (D) and wrinkled surface (E), and cytoskeleton (red) and DAPI (blue) shows cells have clearer alignment parallel to wrinkle with surface topography. (F)(G) Comparison of cell alignment between before wrinkle formation and after wrinkle formation. After wrinkle formation (G), cells show better alignment[58].

1.2.3. Dynamic Change of Cardiomyocyte on Shape Memory Polymer

It has been proven by previous studies that surface topography will strongly affect cell shape and morphology, and on different surface topography, cells exhibit different condition, such as increasing proliferation on nanofiber[56] and stronger adhesion on nanopillars[44]. Based on previous work, researchers try to seed cells on dynamic surface to discuss response of cell to surface changes and mechanism of cells transfer to another condition. Wang's team shows hASCs will improve their alignment on tBA substrate during wrinkle formation[44]. Conversely,

Davis's team used NOA63 as material to make SMP with ability to recover the wrinkle surface back to flat. On their SMP, mouse embryonic fibroblasts show alignment with same direction, but cell alignment becomes disorder and random after polymer shape change and wrinkle disappeared[70]. Surface topography, including wrinkled surface, influences the alignment and orientation of cardiomyocytes, which is important to function of cardiomyocyte[45]. However, previous work focused on the static surface topography to achieve the cell alignment but did not demonstrate the dynamic response of cardiomyocytes to the changes of surface topography.

The shape memory polymer provides an opportunity to study the dynamics of cardiomyocyte alignment according to the surface topographic changes. During the polymer shape recovery, the surface topography will change to induce mechanical stimulation to the cardiomyocytes cultured on the top of the polymer. The response of the cardiomyocytes is observed both in brightfield and florescence for measurement of morphological changes, such as alignment direction change or elongation change.

2. Materials and Methods

2.1. Overview

We used shape memory polymer to create dynamic surface topography. Based on this dynamic surface, we can study the response of cardiomyocytes to the topography change. Thus, the whole process has three steps: including polymer preparation, cells preparation, polymer recovery, and data collection and analysis, shown in **Figure 17**.

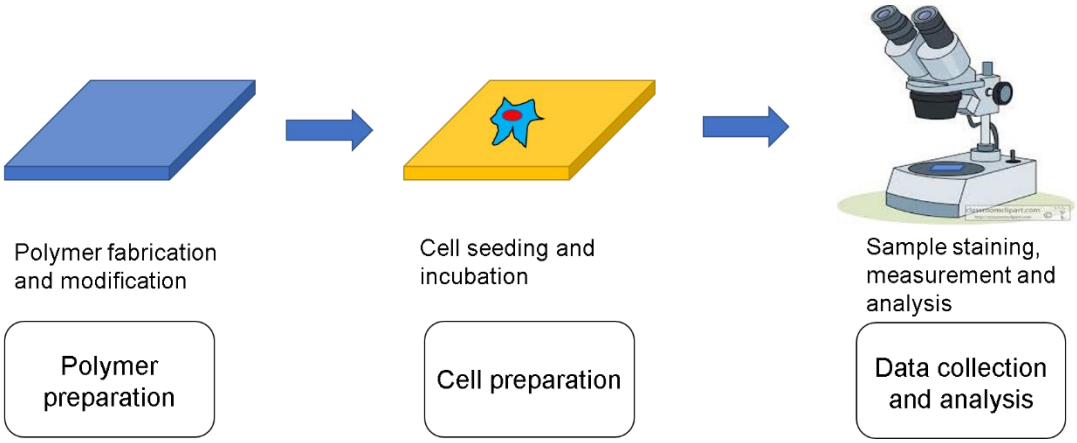

Figure 18 The experimental process, including polymer preparation, cell preparation, and data collection.

To set up the shape memory polymer system, we used Tert-Butyl Acrylate (TBA), since this polymer has the ability to change and recover its shape at a low temperature, ensuring the cells survival on the surface. The polymer is fabricated, stretched, and coated for cell seeding. Next, for cell preparation, we seed cardiomyocytes on the polymer surface at a low temperature, which avoids the polymer shape change. In this step, the purpose is to allow the attachment and spreading of cardiomyocytes on the surface. Last, we increase the temperature to induce the polymer shape recovery and formation of a wrinkled surface. At different time points after starting recovery, we collect and analyze the data of cardiomyocyte responses.

2.2. Polymer Preparation

2.2.1. Polymer Fabrication

The main component of the polymer is Tert-Butyl Acrylate (TBA), which has abilities to fully recover to its original shape. The monomer solution is prepared at 95 percent weight TBA and

5 percent weight Butyl acrylate (BA) with 1 percent weight 2-2-dimethoxy-2-phenylacetophenone (DMPA) of total weight of TBA and BA, as the initiator, and Tetraethylene glycol dimethacrylate (TEG DMA), as the crosslinker, according to the manufacturer's instructions shown in the equation below:

$$\text{Volume in mL of TBA needed} = \frac{(\text{Mass of DMPA in grams}) * (\text{weight percent of TBA})}{(\text{density of TBA})}$$

$$\text{Volume in mL of TBA needed} = \frac{(\text{Mass of DMPA in grams}) * (\text{weight percent of BA})}{(\text{density of BA})}$$

The density of TBA is 0.875 g/ml, and the density of BA is known as 0.894 g/ml. The volume of TEG DMA is the same as the volume of BA. For instance, 25 mg DMPA can produce 2.968 ml TBA and BA solution, which needs 2.714 ml TBA, 0.127 ml BA, and 0.127 ml TEG DMA.

After the TBA solution has been fully mixed, TBA and BA solution was then added into the polymer fabrication mold (**Figure 18**). The mold includes two glass slides, Teflon spacers, and several binder clips. The inner sides of the glass slides need to be coated by Rain-X to make it hydrophobic and to avoid crosslinked polymer adhering to the glass. Teflon was cut to match the size of the glass slides and fixed between the two glass slides by the binder clips. The number of binder clips depends on the size of the glass slides and the size of the binder clips. The binder clips should be enough to cover the entire mold to avoid polymer solution leakage.

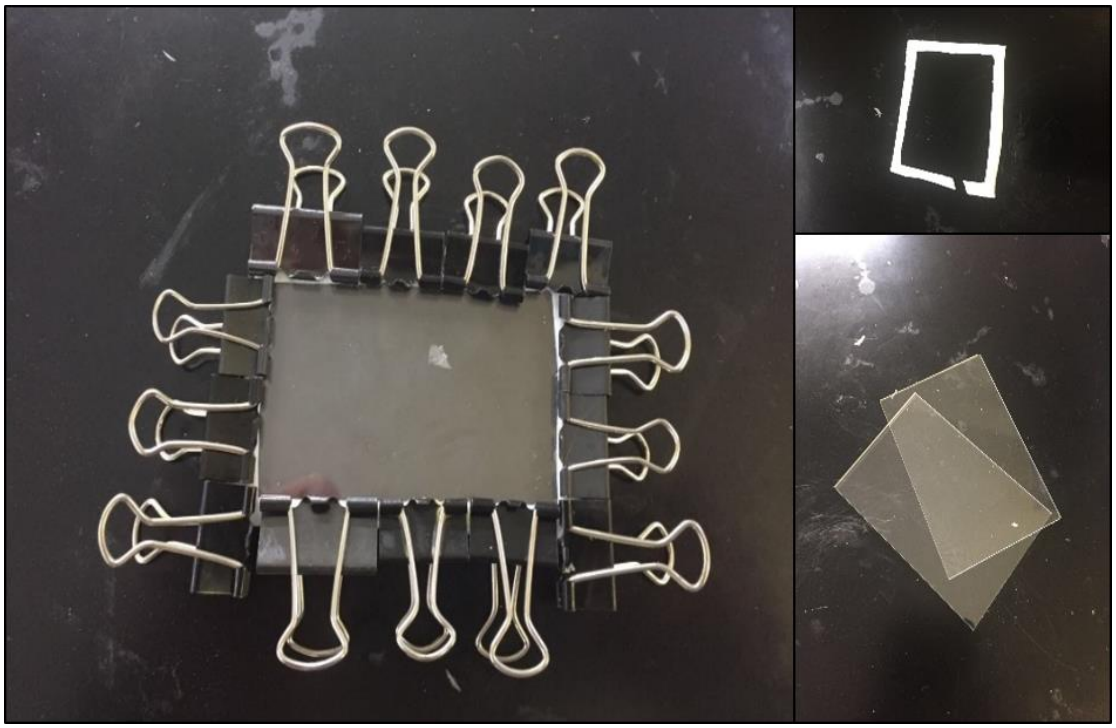

Figure 19 Polymer fabrication mold consists of two glass slide layers, Teflon spacer, and binder clips. The right images are one Teflon spacer and two glass slides.

After TBA solution was added into the mold, the entire mold was moved into the ultraviolet light (UV) box to photo-crosslink for 1 hour. After crosslinking, the polymer is taken out from the mold and put into the 50% methanol solution with deionized water (DI water). Methanol solution with polymer is placed onto a shaker over six hours to extract the residual TBA and BA monomers from polymer. After washing, polymer is taken out of the methanol solution, placed into a hood for drying over six hours, and then put into a vacuum oven for drying over six hours at room temperature. Finally, the polymer is taken out of the oven and ready for use.

2.2.2. Polymer Stretching

For stretching, polymer is cut into small pieces with a length of 2.3 cm and a width of 0.5 cm to match the size of the stretcher. Stretching can be done both automatically or manually

(**Figure 19**). For automatic stretching, Dynamic Mechanical Analysis (DMA) is used to stretch the polymer to 140 % of original length according to the program. For manual stretching, one small piece of polymer is fixed on the manual stretcher by its two clips, and the screws are tightened to apply ~3N force to avoid polymer falling or breaking. Oven is preheated to 70°C, and the stretcher with polymer is moved into the oven to heat the polymer for five minutes. When the polymer becomes softer, it is slowly stretched by rotating the knob of the stretcher to 140% of original length. After finishing the stretching, the stretcher and polymer are taken out of the oven and cooled to room temperature, and the polymer is now ready for spin coating.

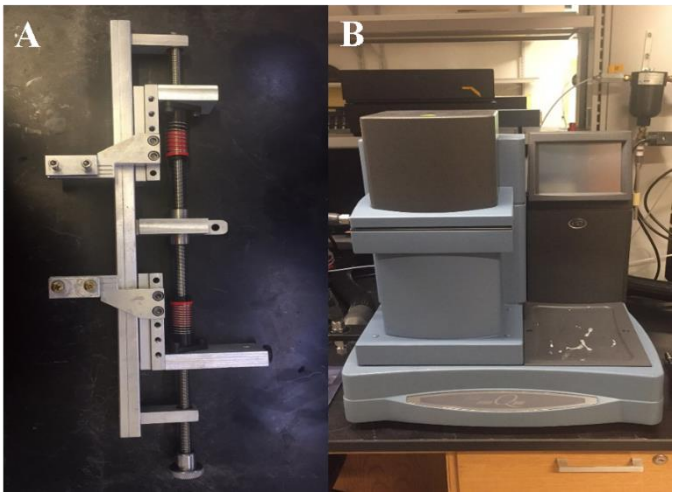

Figure 20 Manual stretcher and DMA for polymer stretching.

2.2.3. Polyelectrolyte Multilayers (PEM) Film Deposition

The formation of winkles on the polymer surface is based on the folding of PEM film due to the shortening of polymer which occurs when the stretched SMP recovers to its original shape. PEM film includes a layer of PEI coating, 20 layers of PSS coating, 20 layers of PAH coating, and 80 times water rinse. Polymer is fixed in the center of spin coater (**Figure 20**) by two-sided

tape. For PEI coating, PEI solution is added to the polymer by the dropper pipette to cover the entire surface of polymer, and spin-coated for 12 seconds at 3000 PRM. After PEI coating, it is 20 times bilayer coating, which includes a layer of PSS coating, two times water rinse, a layer of PAH coating, and two other times water rinse. The spin coating for each layer is 12 seconds at 3000 PRM.

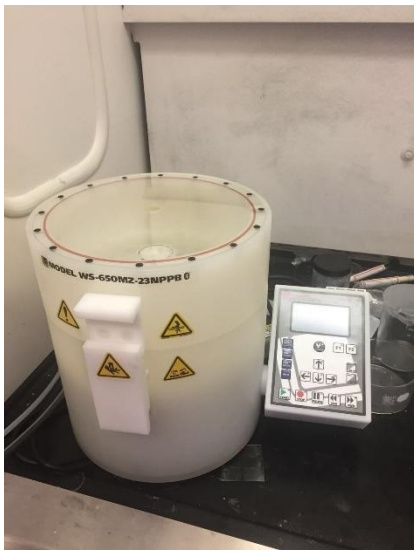

Figure 21 The PEM film is coated onto the stretched polymer in the spin coater.

2.2.4. Geltrex Coating

For attachment and growth of cardiomyocytes, the polymer needs to be coated with Geltrex. After the polymer is coated by PEM film, it is cut into smaller pieces with the size suitable to single well of 48-well plate. Small pieces of polymer are moved into 48 wells plate and incubated with Geltrex solution (normally less than 500 µl) with PEM film side facing to the solution. The polymer in the 48 wells plate is placed at room temperature overnight, and it is ready for cell seeding on the second day.

2.3. Cell Preparation

2.3.1. Cell Culture

We used cardiomyocytes derived from human induced pluripotent stem cells (hiPSC-CMs). hiPSC-CMs are cultured in the wells plate in a 37°C incubator with 5% CO_2 and maintained in RPMI media supplemented with B-27 complete (RPMI-B27). The media needs to be refreshed every two or three days.

2.3.2. Cell Seeding

After polymer surface coated with Geltrex for one day, the polymer is ready for cell seeding. hiPSC-CMs are washed with a PBS solution and incubated with 0.025% trypsin at 37°C for 5 to 10 min to detach the cardiomyocytes from the bottom of the plate. EB20 media is warmed up to 37°C in the water bath and added into cell suspension to stop the function of trypsin. Cell suspension is transferred into a tube and centrifuged at 800 RPM for 5 minutes. Supernatant is aspirated after centrifuge and re-suspended with RPMI-B27 media. RPMI-B27 media should be warmed up to room temperature, instead of in a water bath, to avoid polymer recovery in the latter steps. Hemocytometer is used to count cells of suspension. Rock inhibitor is added into cell suspension to make 10 nM concentration solution.

Based on the cell counting, 30,000 cells are seeded into each well of a new 48 wells plate. This optimized cell number ensures enough cell growth on the polymer surface to avoid the

formation of clusters with too many cells. Additional RPMI-B27 media is added into each well to 700 µl media. For instance, if the cell density of cell suspension is 90,000 cell/ml, 333 µl should be added into one new well to have 30,000 cells, and 367 µl RPMI-B27 media need to be added into the same well. Next, one small piece of polymer is moved into the well with cell suspension, and the side with PEM film should face the media. After cell seeding, the 48 well plate is incubated at 30°C with 5% CO_2 to avoid polymer recover.

2.4. Data Collection

2.4.1. Rising Temperature and Polymer Recover

Cardiomyocytes will attach and spread on the surface after a two day-culture at 30°C. Next, the cell culture plate is transported to a 37°C incubator with 5% CO_2 to trigger the polymer recovery. At the beginning of the temperature increase, the initial time point is set as 0 hour. One polymer is taken out of the cell culture plate every 4 hours from 0 hour to 24 hours, which gives a total of 7 polymer samples set as 0h, 4h, 8h, 12h, 16h, 20h, and 24h. After the polymer is taken out, it is washed three times with PBS solution immediately, fixed with 4% PFA solution for 20 minutes, and washed again three times with a PBS solution. Finally, the polymers and cells are fixed stored in a PBS solution at 4°C in fridge.

2.4.2. Immunostaining

Through the fluorescent labeling on different proteins in the sarcomere and myofibrils, we can observe and identify different components and structures of the cardiomyocytes. In this

experiment, α-actinin, F-actin, myosin heavy chain, vinculin and nucleus are used to visualize the alignment of cardiomyocytes and the organization of sarcomere with antibodies staining. Samples were separated in groups, and each group has seven samples. Samples were fixed at different time from beginning of rising temperature to 24 hour, and every two samples have a 4 hours gap, including 0h, 4h, 8h, 12h, 16h, 20h, and 24h. At different time points, one sample is taken out from 48 well plate and washed with PBS solution by three times. After PBS solution washing, the sample is fixed by 4 % PFA solution, and 0.2% triton solution is added into wells to cover the polymer for five minutes after washing three times with PBS solution. 2% BSA solution is used instead of a triton solution and cover samples for 30 min. After removing the BSA solution, polymers were incubated with primary antibodies for labeling α-actinin, myosin and vinculin for 2 hours, washed with PBS three times, and incubated with secondary antibodies for 1.5 hours. For actinin and vinculin staining, both primary and secondary antibodies are diluted to 100 folds, and for actin staining, antibodies are diluted from 7 μl to 50 μl without primary antibody. After the polymer is washed three times by PBS, DAPI solution is used to stain the nucleus for 10 minutes.

2.4.3. Measurement and Analysis

Fluorescent images of cardiomyocytes are captured using a 40x oil objective on a Nikon microscope. Each polymer is imaged with at least five positions with the brightfield channel and all stained fluorescent channels. The brightfield images are used to determine the condition and orientation of wrinkles, and the fluorescent channels are used to determine the different components of the cardiomyocytes.

Cardiomyocytes with clear sarcomere structures are the main targeting cells for measurement. The cell area is determined by manually drawing a line surrounding the cardiomyocytes. To determine the cell elongation, an entire individual cardiomyocyte is surrounded by a rectangle, and the ratio of length and width of the rectangle (aspect ratio) determines the anisotropic cell elongation. To determine the nuclei elongation, an entire nucleus of an individual cardiomyocyte is surrounded by a rectangle to calculate the aspect ratio of the cell nucleus. To determine the cell and nuclei orientation of individual cardiomyocytes, the angle between wrinkle direction and length of cell rectangle or nuclei rectangle is measured. A smaller angle indicates better alignment of cardiomyocyte along the wrinkle directions.

The length between two Z-discs (α-actinin staining) is considered as the length of sarcomere. Each cell will be chosen six random positions for sarcomere length measurement, and each image was chosen 3-5 cells (**Figure 21**). Thin filament (F-actin staining) and thick filament (myosin staining) are measured based on length, width, and direction by using the rectangles similar to the method for cell and nuclei measurement. Focal adhesion costamere (vinculin staining) is measured at the edge of individual cardiomyocytes based on overall size. The Z-disc is measured from six different positions in each single cardiomyocyte, while F-actin, myosin, and vinculin are measured from four different positions (**Figure 22**).

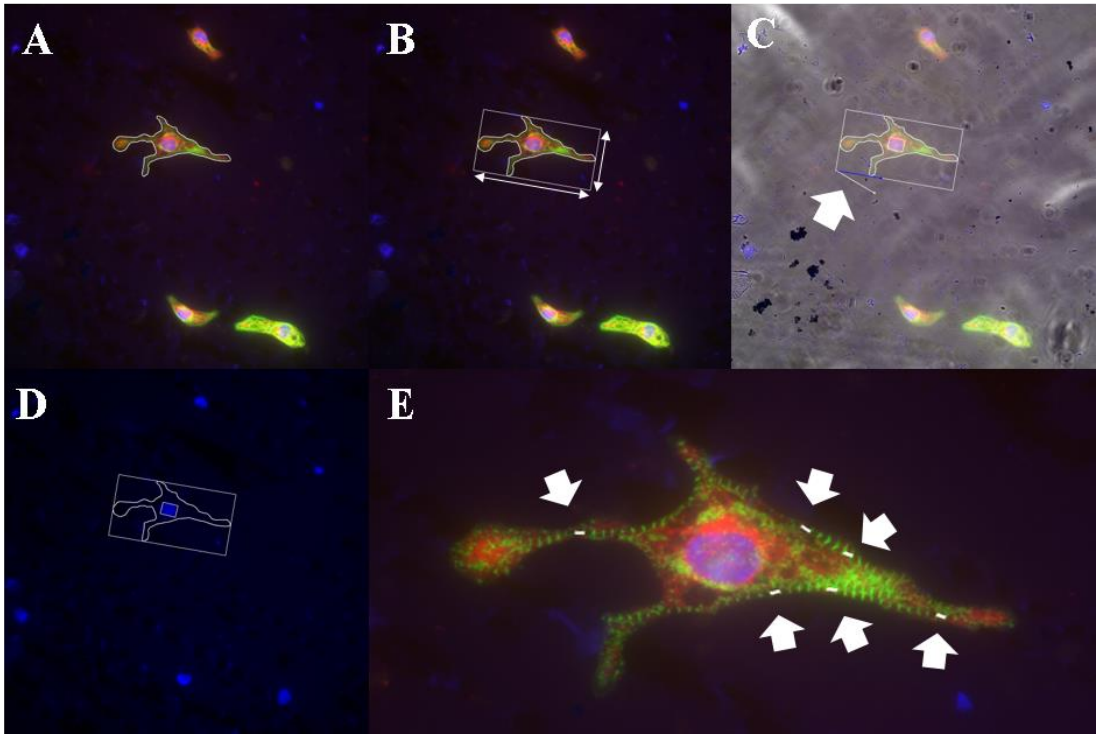

Figure 22 Measurements of cardiomyocyte morphology and sarcomere length. (A) Cell area of the cardiomyocytes under fluorescence. (B) Rectangle is used to measure the aspect ratio of cell elongation. (C) The angle between wrinkle and rectangle is measured as cell orientation. (D) Based on the same method with rectangle, nuclei elongation and orientation are also measured. (E) 6 positions are selected for sarcomere measurement for each individual cardiomyocyte.

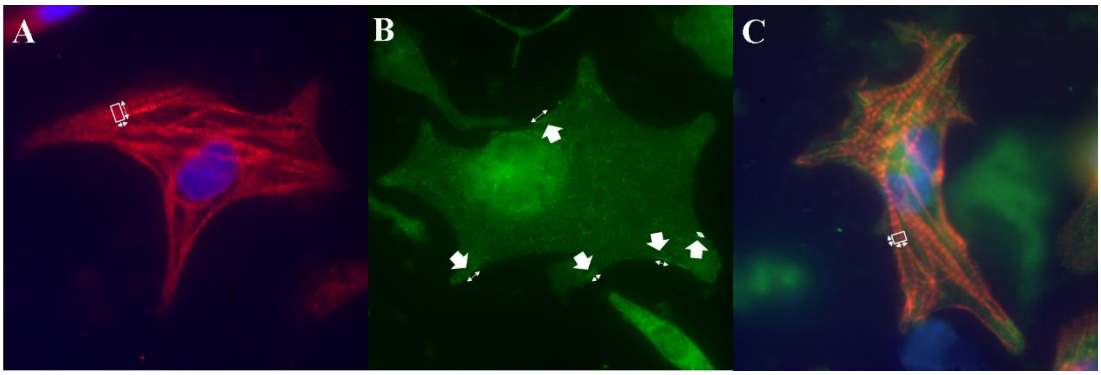

Figure 23 Measurements of myosin, vinculin and actin. (A) Using rectangle to surround myosin (red) to measure length and width. (B) Vinculin (green) was measured in length. (C) Similar method for myosin measurement was used for actin (red).

2.4.4 Beating Motion Tracking

Cardiomyocytes beating was recorded by brightfield microscopy as 15 seconds video and was

analyzed by Motion -tracking algorithm with Matlab. Region of interest (ROI) was selected by rectangle box in video frame. The contractile motion velocity was calculated as the average of peaks in waveform plot. Coupled double peak was considered contraction and relaxation peak. Single cell was targeted and selected by rectangle box as ROI.

2.4.5. Statistical Analysis

Data is analyzed using the software Prism 6 (version 6.01). Data was presented as mean with standard deviation (SD) for each time point. One-way ANOVA with multiple t-test is used to compare the difference among different groups. $P < 0.05$ is considered as a significant difference. Angle data is analyzed and plotted using MATLAB with polar-histogram chart to show the orientation at different angles.

3. Results

3.1 Cardiomyocyte Culture on Static Surface

Many previous studies showed that ECM will strongly influence the behavior of cells, and researchers can induce cell alignment in target direction through design and control the topography of the substrate. In 2011, McCain et al showed that the cells had a stronger response to the topography than to an electricity current. By designing the topography with groove and flat, the cells had better alignment on the grooved surface[72]. Moreover, Wang et al showed that the cells had a higher alignment preference on anomalous wrinkled surfaces than on flat surfaces[73]. In our experiment, at first, we seeded cardiomyocytes on the static wrinkled and flat

surface to see if the cardiomyocytes also had a similar response to the surface topography.

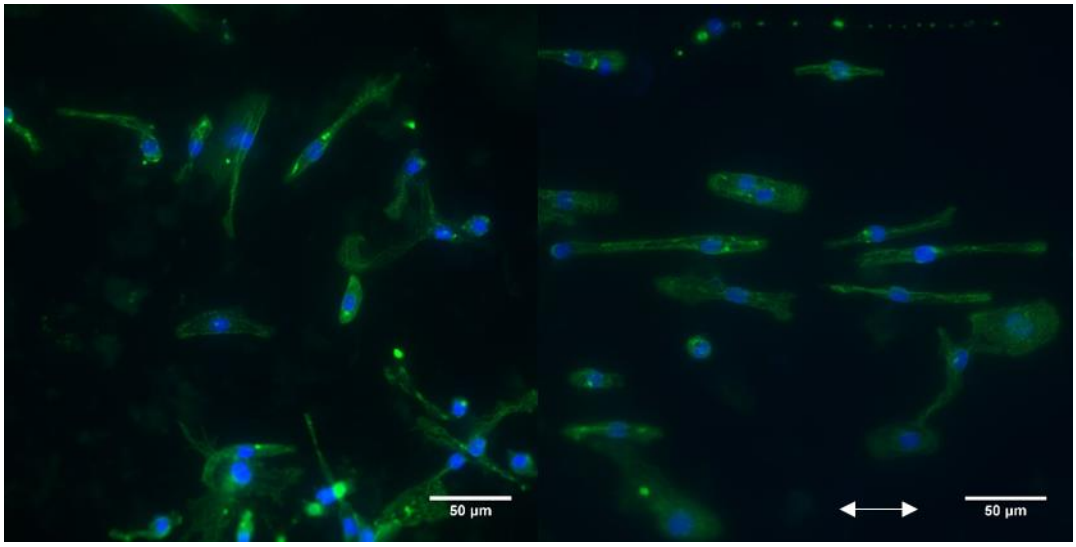

Figure 24 Fluorescence images of cardiomyocytes. Left is flat surface, and right is wrinkled surface. The actinin (green) showed the sarcomere structure and cell nucleus was stained by DAPI (blue). The arrow shows the direction of the wrinkle.

The fluorescence images show that on the TBA polymer with PEM film, the cardiomyocytes have better alignment on the wrinkled surface. Most cells show a similar alignment direction, parallel to the wrinkle direction (**Figure 23**). In the static surface experiment, we selected 20 cells from both the wrinkled surface group and the flat surface group respectively. On the flat surface, cardiomyocytes align randomly into the directions with large range of angle distribution, and only 5% of total cells are in the range from -15° to 15° to the horizontal direction parallel to the wrinkle direction. On the wrinkled surface, the angles of most cells are in the range from -15° to 15°, account for 75% of total number of cells (**Figure 24 and Table 1**). For the cell shape (**Figure 25**), it also shows significant difference between the flat surface and the wrinkled surface with the *p*-value of 0.0006. The cells seeded on the wrinkled showed a much higher aspect ratio than the cells on the flat surface.

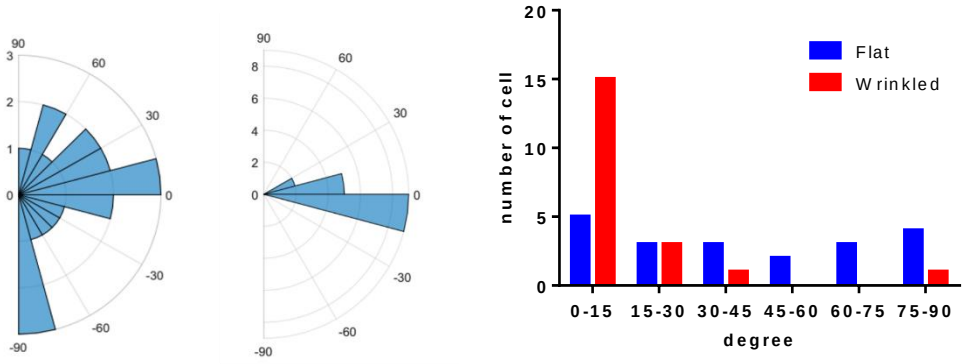

Figure 25 Number of Cells seeded on topography with angle distribution. On the flat surface, angles of cell orientation are randomly distributed in range from -90° to 90°. On the wrinkled surface, the angles are closer to 0°.

Table 1 Angle distribution within -15° ~ 15° of cell alignment on polymer surface**.**

	Flat surface	Wrinkled surface
Number	5 cells	15 cells
Portion	25%	75%

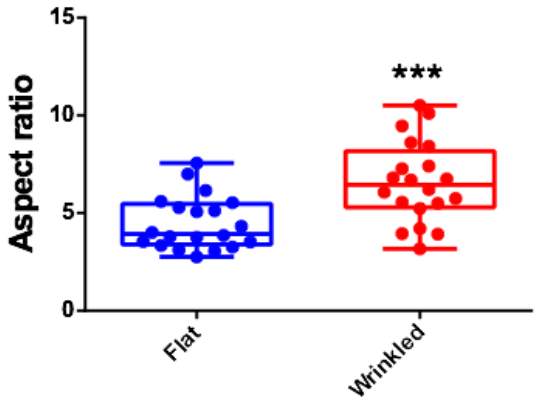

Figure 26 Aspect ratio of 20 cardiomyocytes aligned on each different topography. On the wrinkled surface, the cardiomyocytes showed a more elongated cell shape than on the flat surface. *** *p* value = 0.0005

3.2 Polymer Recover and Wrinkle Formation

Compared to previous research on cardiomyocyte alignment on the static topographic substrate, the uniqueness of our research is that cardiomyocytes grow on a dynamic surface, which requires surface change with living cells. The entire experiment was controlled in a certain narrow range temperature from 30° C to 37° C. During cell seeding and spreading on the SMP before shape recovery, the temperature needs to be controlled to not allow recovery and wrinkle formation, but still keep cellular normal behaviors. During the wrinkle formation, the temperature needs to be controlled to quickly form the wrinkles but not damage the cell viability.

Polymers were tested for shape recovery at different temperatures. At 30° C, polymer did not show any shape recovery, and there is no clear wrinkle on the surface. At 33° C, it shows some, but not clear wrinkles on the surface. At 37° C, wrinkle formation can be observed in 1 hour, and it became clearer within 2 hours. At 42° C, the wrinkle formed after only half an hour. Therefore, 30° C was chosen as the initial cell culture temperature, and 37° C as the recovery temperature. During cell seeding and culturing at 30° C, there is no wrinkle formation on the polymer surface. Raising the temperature up to 37° C, wrinkles quickly formed on the surface. After 1 hour at 37° C, we observed clear wrinkle formation on the surface, and after 2 hours, the wrinkles covered the entire surface of polymer.

3.3 Cardiomyocyte Morphology Changes

Next, cardiomyocytes were seeded on the polymers at 30° C for two days, and then the polymers were placed at 37° C for recovery. The samples were collected every 4 hours till 24 hours, which resulted in a total of seven sample groups, including 0, 4, 8, 12, 16, 20 and 24 hours. With the staining of actinin and actin, it shows cardiomyocytes have clear sarcomere structure during polymer recovery (**Figure 26**). However, the orientation of cardiomyocytes has been influenced according to the results of orientation angle of the cells. The clear sarcomere structure indicated that polymer recovery did not damage the entire cells, and cells could adjust their alignment by cytoskeletal rearrangement.

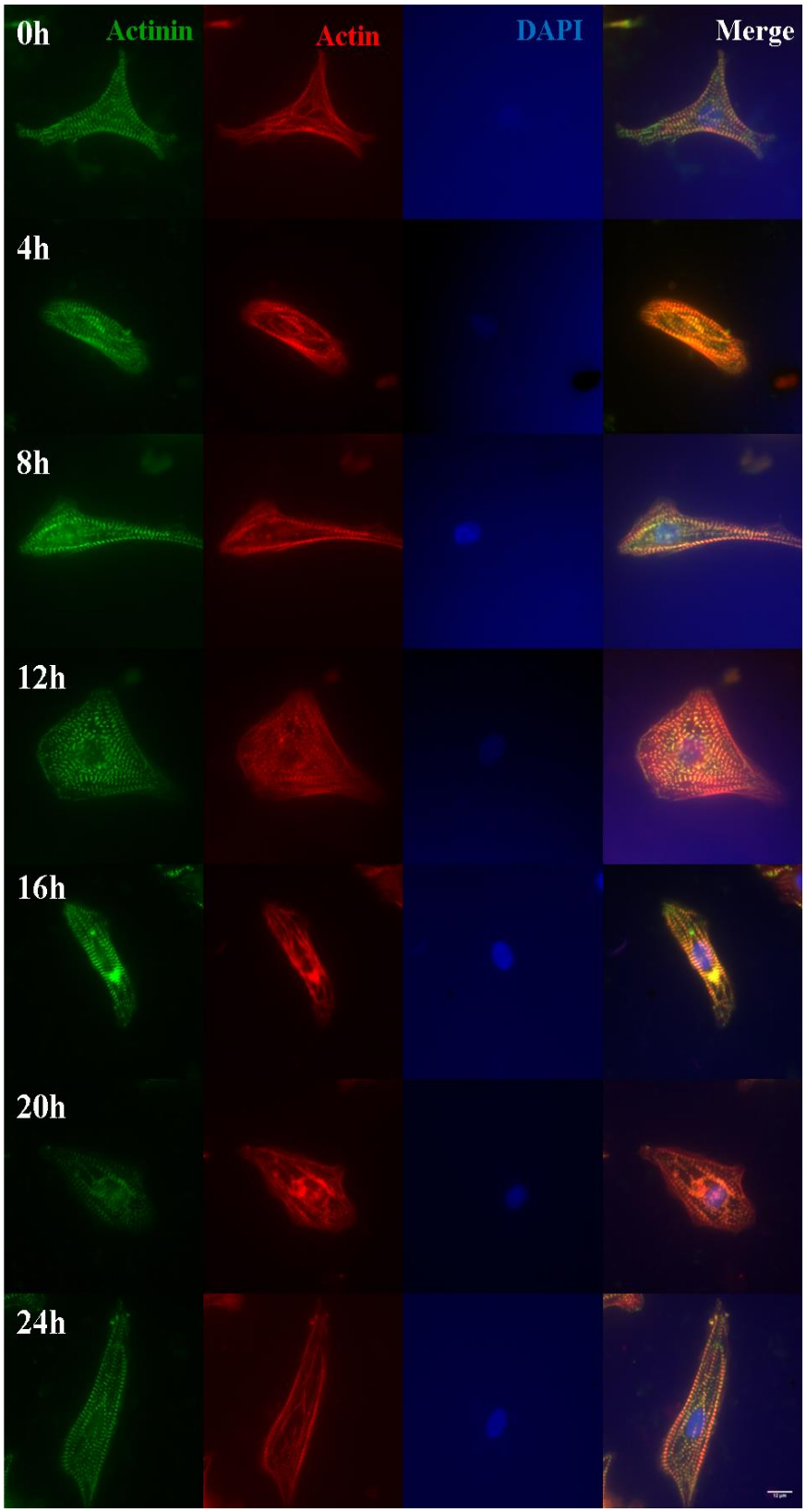

Figure 27 Fluorescence staining of cardiomyocytes at different time points, including actinin (green), F-actin (red) and DAPI (blue). At different time points, cardiomyocytes all show clear sarcomere structure.

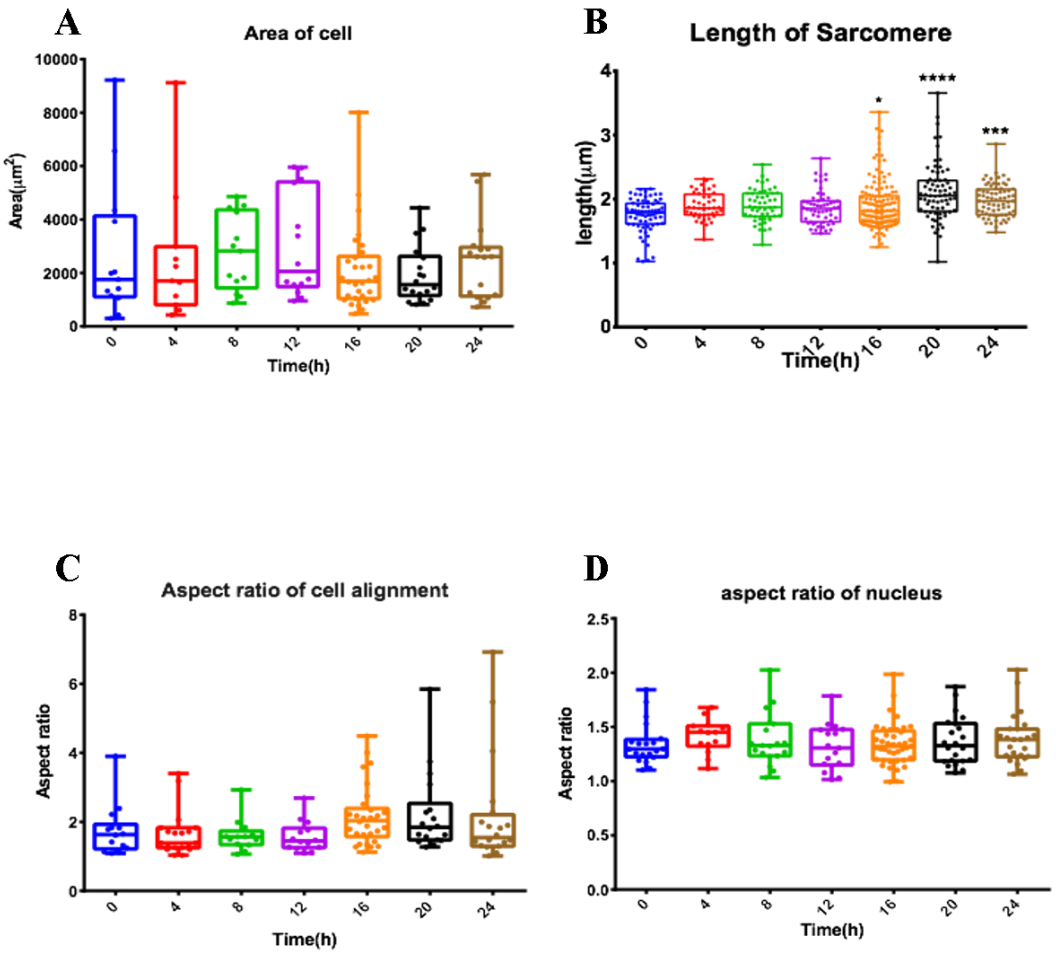

Figure 28 Morphology results of cardiomyocytes on the dynamic surface. (A) Area of cardiomyocytes on the dynamic surface at different time points, showing no difference. (B) Length of sarcomere at different time points shows significant difference from 16 hours to 24 hours (*p*-values are 0.0123, < 0.0001 and 0.0002). (C)(D) Aspect ratio of cell shape and nucleus shape did not show significant difference.

The cell area is usually used to show the condition of cells spreading, so we studied the cell area of cardiomyocytes to determine the influence of wrinkle formation on the cardiomyocyte spreading. From the results, we find that the area of cardiomyocytes shows high variations even within different time points. Within 24 hours after polymer recovery, it does not show any trend of changes of cell area (**Figure 27A**). Although the staining of actinin and F-actin shows that the sarcomere structure is not disassembled, when cardiomyocytes respond to the wrinkle formation, the length of sarcomere is increasing from 16 to 24 hours (**Figure 27B**).

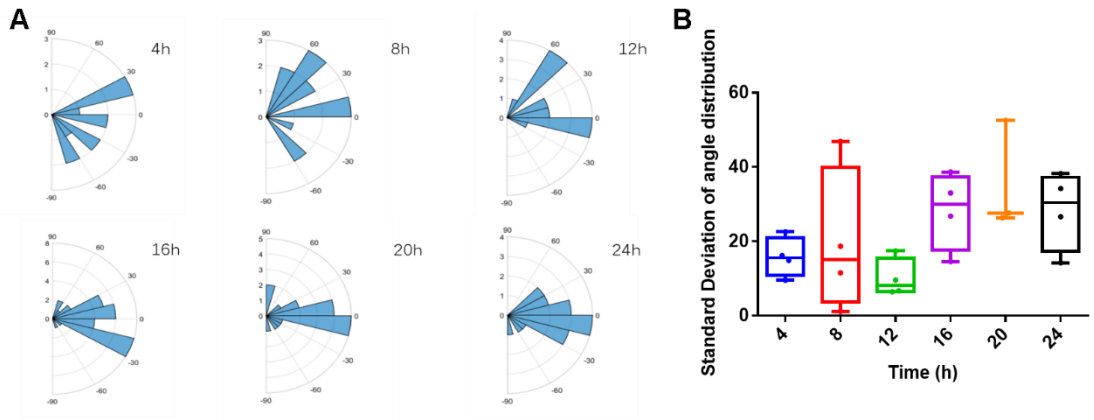

Figure 29 Angle Distribution of Cardiomyocytes alignment. (A)Polar-histogram of angle between cell orientation and wrinkle at different time points. The angles are randomly distributed from 90° to -90° at early time points, but close to 0° at later time points. (B) Standard Deviation of cardiomyocytes angle between alignment and wrinkle.

Table 2 Percentage of cells with angles between cell orientation and wrinkle smaller than 15° on dynamic surface

Time (h)	4	8	12	16	20	24
Percentage (%)	27	23	24	33	50	41

As previously mentioned, cell angle and shape (aspect ratio) show the level of cell alignment. We measure the aspect ratio and orientation angle between the cardiomyocytes and wrinkle at different time points. In **Figure 28**, the angle distribution does not show any preference in the first 12 hours, but slowly aggregates close to 0° till 24 hours. In **Table 2**, it shows that the percentage of orientation angles smaller than 15° increases after 16 hours. For the aspect ratio of cardiomyocyte shape, within 24 hours, it does not show significant difference at the different time points. However, after 16 hours, some cardiomyocytes show high aspect ratio in their shapes in the latter three groups (**Figure 27C**). It might indicate that the 16th hour can be an important time point, when the cardiomyocytes respond to wrinkle formation. Additionally,

the nucleus orientation and shape can be also used to investigate the cell alignment. Compared to the cell alignment, the nucleus orientation shows no significant changes within 24 hours. Moreover, the aspect ratio of the cardiomyocyte shape shows an increase at 16 hours, but aspect ratio of the nucleus still remains the same level without any change.

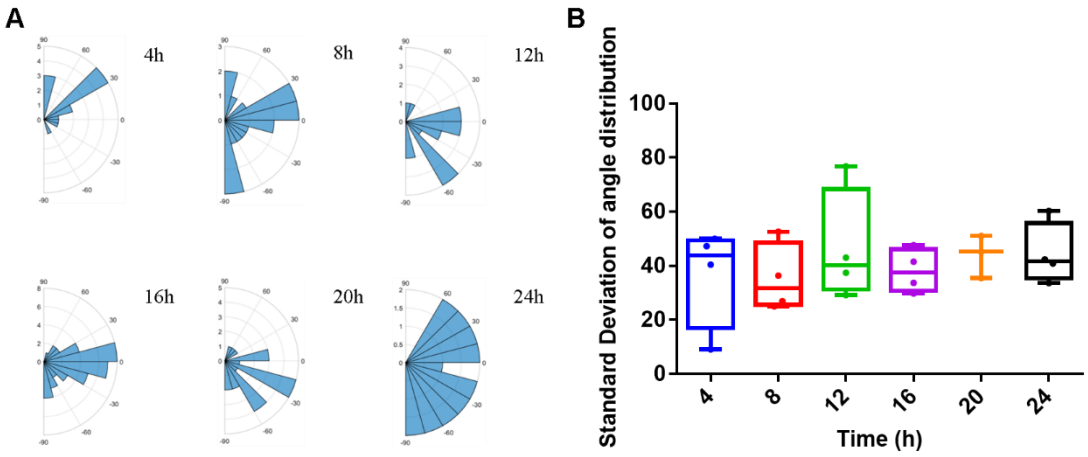

Figure 30 Angle Distribution of Cardiomyocytes Nucleus. (A) Polar-histogram of angles between nucleus orientation and wrinkle at different time points. For all the time points, results did not show significant changes, and angles randomly distributed in the range from 90° to -90°. (B) Standard Deviation of cardiomyocytes angle between nucleus and wrinkle.

Table 3 Percentage of cells with angles between nucleus orientation and wrinkle smaller than 15° on dynamic surface

Time (h)	4	8	12	16	20	24
Percentage (%)	14	26	35	36	15	19

3.4 Cardiomyocyte Sarcomere Structure Changes

Cardiomyocytes adhere and align on the surface through the adhesion model, which is

consisted by multiple proteins, such as integrin, vinculin, and cytoskeletal proteins[25]. It is necessary to analyze the change of these proteins to understand the cytoskeletal dynamics of cardiomyocyte reorganization. Actin is the main component of the thin filament, which shows the structure of myofibrils. From staining (**Figure 26 & 31**), actin shows an increasing trend of I band length, during the cell organization starting from 8 hour (**Figure 30A**). Comparing with 7 different time points, thin filament length shows significant difference with *p*-value of 8, 12, 16, 20 and 24 hour with respectively 0.0032, 0.0005, 0.0012, < 0.001 and < 0.0001. However, during the reorganization of cardiomyocytes, the length of myosin does not show any difference at different time points, indicating that A band remained the same during the myofibril remodeling (**Figure 30B & 32**). Vinculin is an important component of costameres, which are related to cardiomyocyte adhesion on the substrate surface. Form fluorescence image, vinculin shows early changes at the 4th and 8th hour with more small scattered spots, but large mature shape at other time points (**Figure 31**). At the 4 and 8 h, the length of vinculin shows significantly decrease with *p*-value < 0.0001 (**Figure 30C**). After 8 hours, the length of vinculin starts to increase and recovers to the original level.

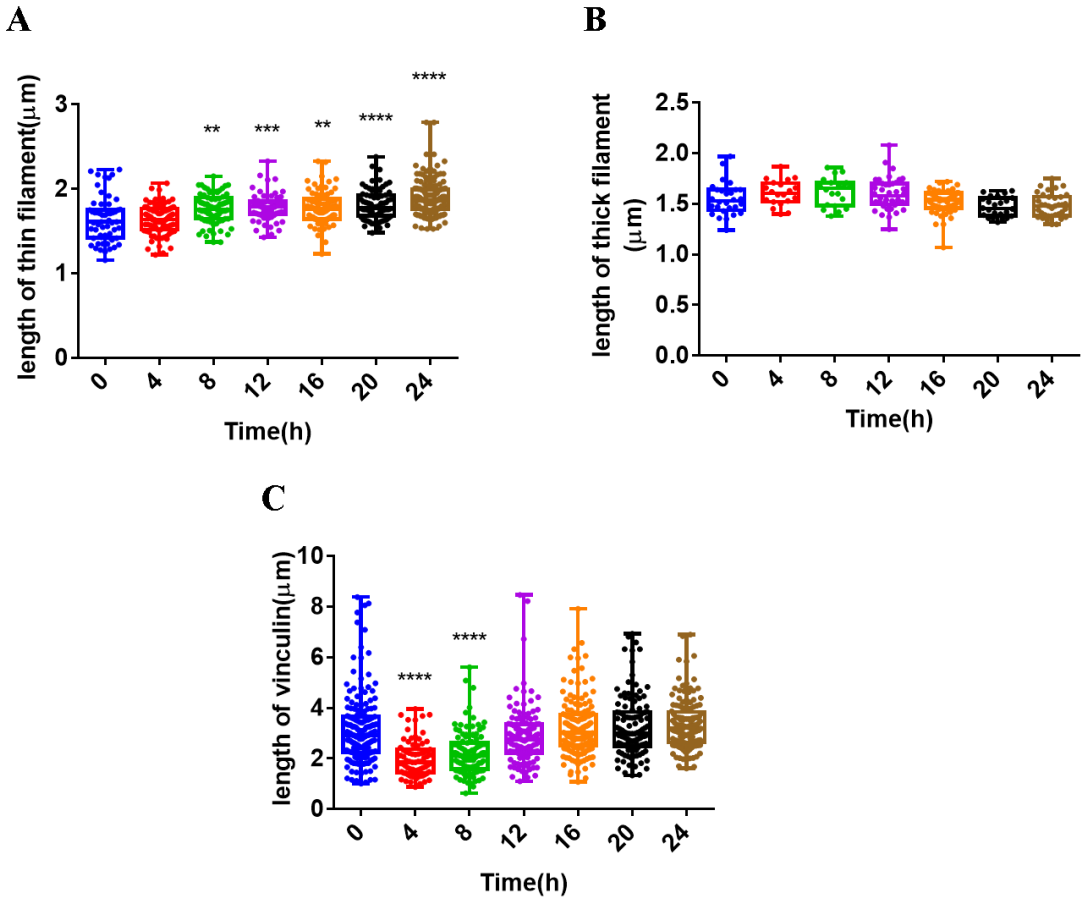

Figure 31 Length results of three important structural components of cardiomyocyte myofibrils, including actin (A), myosin (B) and vinculin (C). (A) Actin shows an increase during the polymer recovery starting at 8th hour. *P*-values are 0.0032, 0.0005, 0.0012, < 0.001 and < 0.0001 (B) No difference of myosin during cardiomyocyte reorganization. (C) Length of vinculin decreases at early time points and increases after 12 hours. *P*- values are < 0.0001 and <0.0001

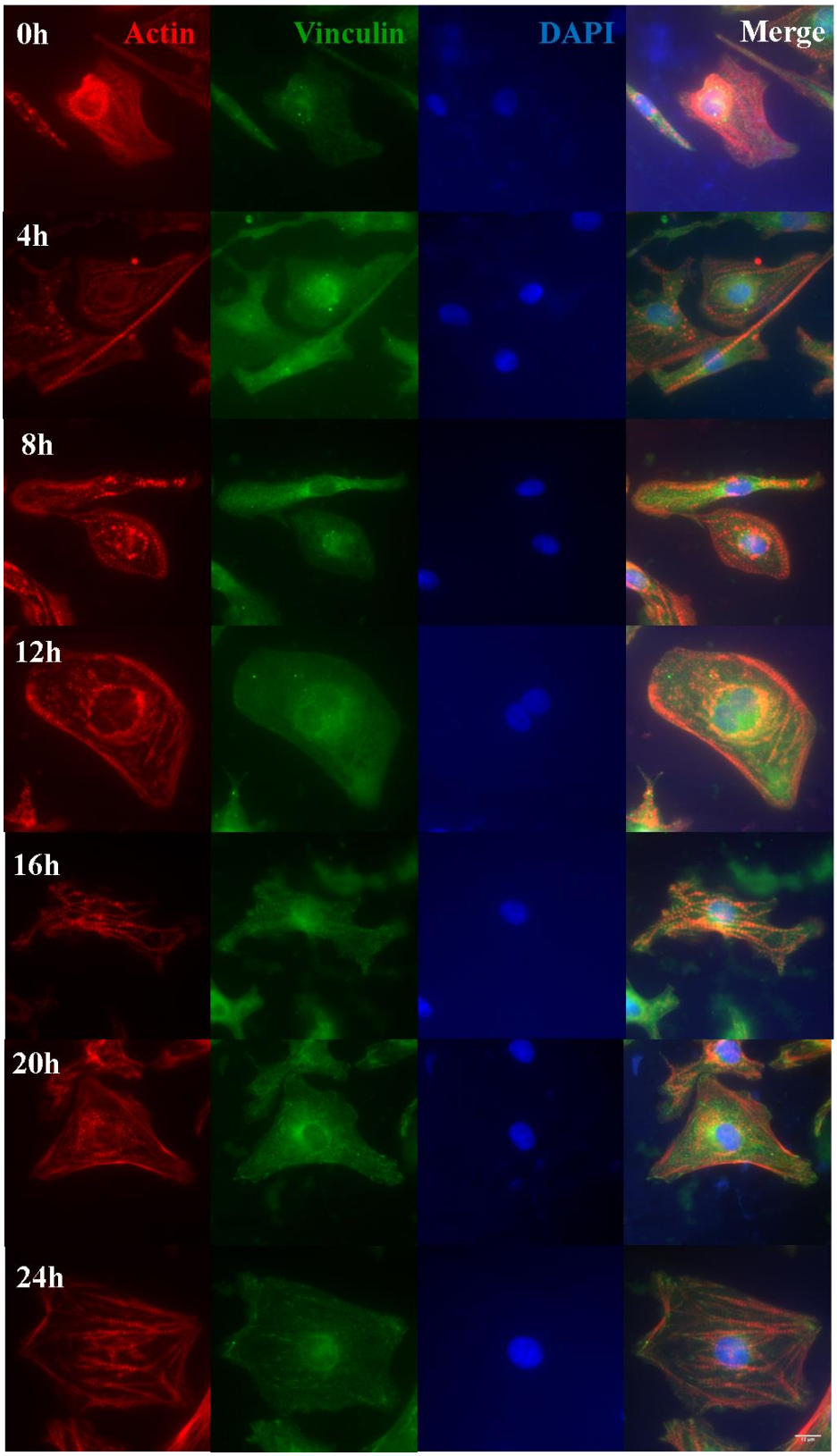

Figure 32 Fluorescence staining of cardiomyocytes at different time points, including actin (red), vinculin (green) and DAPI (blue).

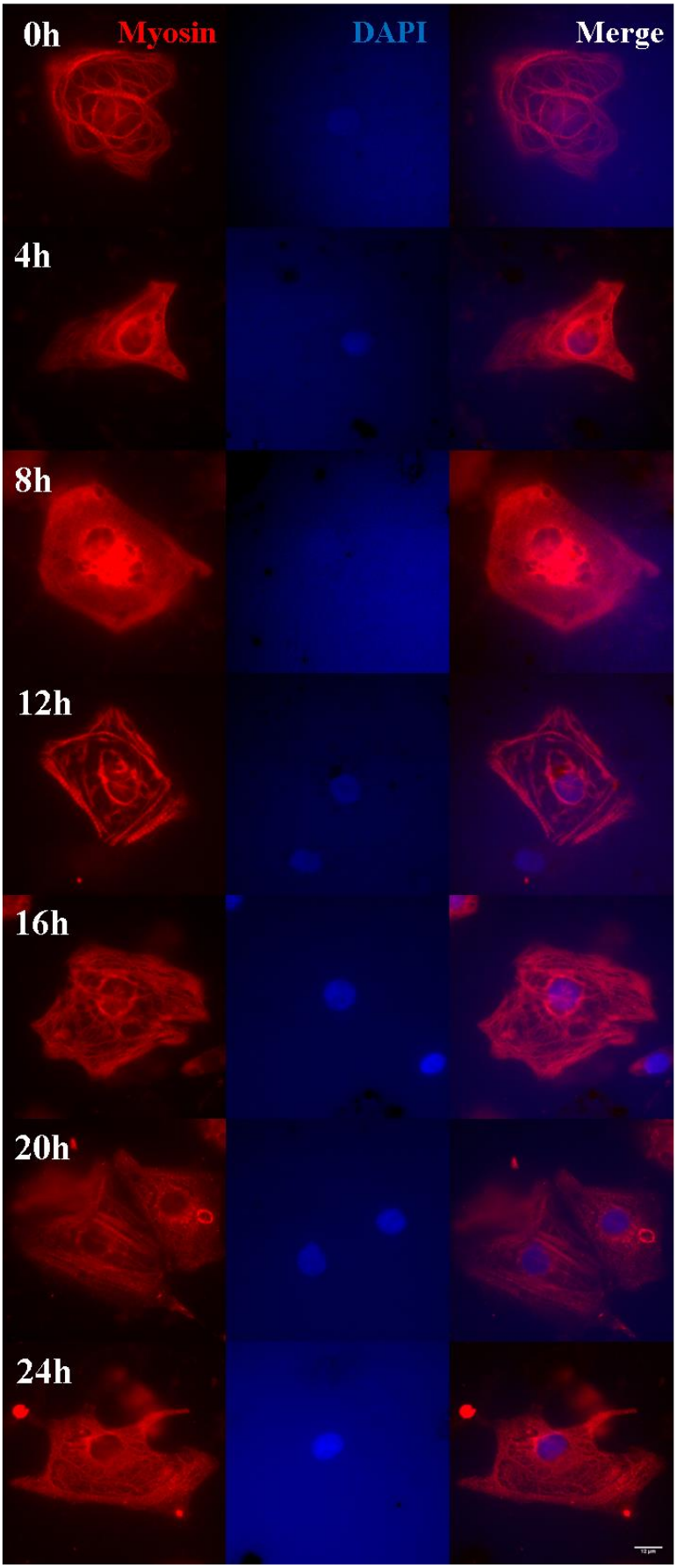

Figure 33 Fluorescence staining of myosin of cardiomyocytes at different time points.

3.5 Cardiomyocytes Beating

In previous research, it has been proved that the integrity and stabilization of myofibril structure is strongly related to cardiomyocyte normal function, and when myofibril structure changes, cardiomyocytes are malfunctioning, shown as lower contraction speed or lower beating rate[74]. In experiment, 8 time points have been selected, including 0, 4, 8, 12, 16, 20, 24 and 36 hours. From the beating rate result, although cell culture was transferred from 30°C to 37°C, it did not show any trend of change (**Figure 34**

A). In addition, interesting, after cell culture was moved to 37°C, contraction velocity did continuously increase, and the beginning and end of time points shows slightly higher than middle time points. Related to previous work, in the first and last time point, the higher function might be related more integrated myofibril structure, and as wrinkle form on the polymer surface in middle time points, cardiomyocytes remodel myofibril, which triggers contraction velocity decrease.

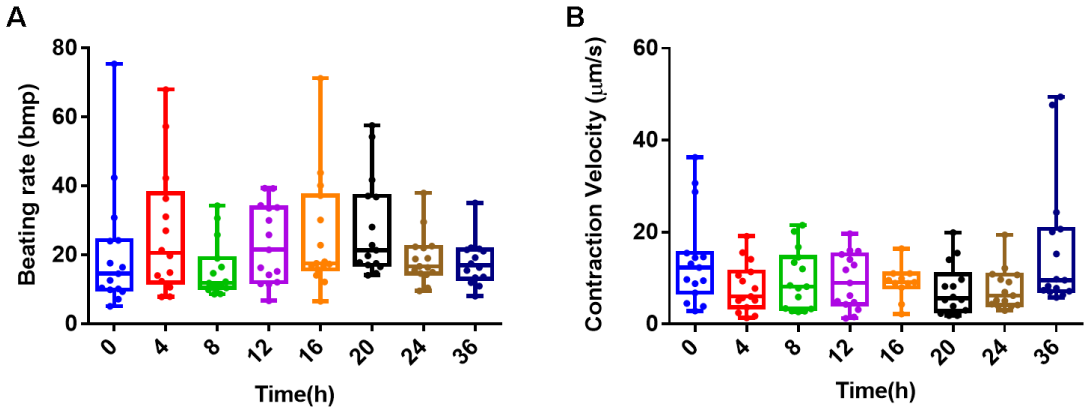

Figure 34 Cardiomyocytes beating analysis. (A) Beating rate of cardiomyocyte, including 8 times points. (B) the contraction velocity of cardiomyocytes.

4. Conclusions

Cardiomyocytes are highly affected by the surface topography, which improves the alignment of cardiomyocytes along with the wrinkles. TBA polymer is proved to be successfully set up as a dynamic surface system, which ensures that the cardiomyocytes can attach on PEM film and survive with shape change. The cardiomyocytes can be aligned on a static wrinkled surface, compared to a flat surface. We also successfully induce the wrinkle formation with cardiomyocyte on the top of the surface. The wrinkles clearly form in 2 hours, but the reorganization of cardiomyocytes is a long and slow process. From the entire 24 hours experiment after starting the polymer shape recovery, the cardiomyocytes do not show too much changes on the morphology (cell area, cell shape aspect ratio, nucleus angle to wrinkles, nucleus shape aspect ratio), but significant changes on cell angle to the wrinkles, which indicated that the wrinkle formation will have more effects on the cell orientation than cell spreading, and nuclei might take more time to respond to the topographic changes.

When the cardiomyocytes respond to the surface topographic change, the results show that different myofibril components have different response orders. It seems that the changes of sarcomere structure are prior to the cell shape and nucleus shape, which might be the series of changes in order. With the staining of different components of myofibrils, it shows that cells do not dissemble the sarcomere structure during the polymer recovery, but only adjust the alignment though the myofibril reorganization. We find a decrease of vinculin length as early as 4 hours after polymer recovery. The potential process can be that after wrinkle formation,

some surface regions become less suitable for focal adhesion attachment, so the integrins on the cell membrane lose adhesion and then disassemble the focal adhesion complex inside the cells. After new connections form between integrins and the surface along with the wrinkle, it helps vinculin anchor free sarcomere to the membrane, which induces the elongation of the thin actin filaments at 8 hours after polymer recovery. The increase the length of I band would further induce the changes on the actinin structure and increase the length between two Z discs. However, during the entire myofibril reorganization process, the myosin thick filaments show no changes on the length of A band.

5. Future Work

Since the samples of this experiment are taken individually at fixed time points, it is difficult to see how the dynamic changes of the same cells within 24 hours. Moreover, the time gap between two samples is 4 hours, which might be a long time for some fast cell responses. This 4-hour time gap might cause missing of important events to be observed. In our future plan, it is better to set up the automatic microscopy system for time lapse imaging of live cardiomyocytes with different reporters on the dynamic surface, so we can focus on the dynamic changes of only one cardiomyocyte, in order to show the entire picture of cell response. On the other hand, compared with the results from static wrinkled surface, our results from dynamic surface show less alignment of cardiomyocytes resulted from the dynamic wrinkle formation. The potential reason might be the entire response process of cardiomyocytes to the wrinkle formation is much longer than what we predicted. Thus, in our future plan, the time

span of the entire experiment should be prolonged. Finally, during the cardiomyocyte reorganization on the dynamic surface, there will be disassembly of old sarcomeres and production of new sarcomeres, indicating that the expression level of different components will change during this process. In the next plan, we want to investigate the gene expression changes of different components, including some key transcriptional factors, to understand specific responses of cardiomyocytes during the reorganization process.

6. Reference

1. Walker, C. A. & Spinale, F. G. The structure and function of the cardiac myocyte: A review of fundamental concepts. *J. Thorac. Cardiovasc. Surg.* **118**, 375–382 (1999).
2. Marieb, E. N. & Hoehn, K. Human anatomy and physiology. (2010).
3. Sanger, J. W., Ayoob, J. C., Chowrashi, P., Zurawski, D. & Sanger, J. M. Assembly of Myofibrils in Cardiac Muscle Cells BT - Elastic Filaments of the Cell. in (eds. Granzier, H. L. & Pollack, G. H.) 89–110 (Springer US, 2000). doi:10.1007/978-1-4615-4267-4_6
4. Opie, L. H. Heart physiology: from cell to circulation. (2004).
5. Claycomb, W. C. *et al.* HL-1 cells: A cardiac muscle cell line that contracts and retains phenotypic characteristics of the adult cardiomyocyte. *Proc. Natl. Acad. Sci.* **95**, 2979–2984 (1998).
6. Au, Y. The muscle ultrastructure: a structural perspective of the sarcomere. *Cell. Mol. Life Sci. C.* **61**, 3016–3033 (2004).
7. Johnson, L. R. *Gastrointestinal Physiology E-Book: Mosby Physiology Monograph*

Series. (Elsevier Health Sciences, 2013).

8. Dabiri, G. A., Turnacioglu, K. K., Sanger, J. M. & Sanger, J. W. Myofibrillogenesis visualized in living embryonic cardiomyocytes. *Proc. Natl. Acad. Sci.* **94**, 9493–9498 (1997).

9. Markwald, R. R. Distribution and relationship of precursor Z material to organizing myofibrillar bundles in embryonic rat and hamster ventricular myocytes. *J. Mol. Cell. Cardiol.* **5**, 341–350 (1973).

10. Ehler, E., Rothen, B. M., Hammerle, S. P., Komiyama, M. & Perriard, J. C. Myofibrillogenesis in the developing chicken heart: assembly of Z-disk, M-line and the thick filaments. *J. Cell Sci.* **112**, 1529 LP-1539 (1999).

11. Gregorio, C. C. & Antin, P. B. To the heart of myofibril assembly. *Trends Cell Biol.* **10**, 355–362 (2000).

12. Huang, S. & Ingber, D. E. The structural and mechanical complexity of cell-growth control. *Nat. Cell Biol.* **1**, E131 (1999).

13. Khalili, A. A. & Ahmad, M. R. A Review of Cell Adhesion Studies for Biomedical and Biological Applications. *Int. J. Mol. Sci.* **16**, 18149–18184 (2015).

14. Lasky, L. A. *et al.* An endothelial ligand for L-Selectin is a novel mucin-like molecule. *Cell* **69**, 927–938 (1992).

15. Okegawa, T., Pong, R.-C., Li, Y., Hsieh, J.-T. & Others. The role of cell adhesion molecule in cancer progression and its application in cancer therapy. *Acta Biochim. Pol. Ed.* **51**, 445--458 (2004).

16. Perinpanayagam, H. *et al.* Early cell adhesion events differ between osteoporotic and

non-osteoporotic osteoblasts. *J. Orthop. Res.* **19**, 993–1000 (2006).

17. Serhan, C. N. & Savill, J. Resolution of inflammation: the beginning programs the end. *Nat. Immunol.* **6**, 1191 (2005).

18. Sagvolden, G., Giaever, I., Pettersen, E. O. & Feder, J. Cell adhesion force microscopy. *Proc. Natl. Acad. Sci.* **96**, 471–476 (1999).

19. The reaction-limited kinetics of membrane-to-surface adhesion and detachment. *Proc. R. Soc. London. Ser. B. Biol. Sci.* **234**, 55 LP-83 (1988).

20. Bernfield, M., Hinkes, M. T. & Gallo, R. L. Developmental expression of the syndecans: possible function and regulation. *Development* **119**, 205 LP-212 (1993).

21. Gumbiner, B. M. Proteins associated with with cytoplasmic surface of adhesion molecules. *Neuron* **11**, 551–564 (1993).

22. Hynes, R. O. Integrins: Versatility, modulation, and signaling in cell adhesion. *Cell* **69**, 11–25 (1992).

23. Turner, C. E. & Burridge, K. Transmembrane molecular assemblies in cell-extracellular matrix interactions. *Curr. Opin. Cell Biol.* **3**, 849–853 (1991).

24. Pardo, J. V, Siliciano, J. D. & Craig, S. W. Vinculin is a component of an extensive network of myofibril-sarcolemma attachment regions in cardiac muscle fibers. *J. Cell Biol.* **97**, 1081 LP-1088 (1983).

25. Pardo, J. V, Siliciano, J. D. & Craig, S. W. A vinculin-containing cortical lattice in skeletal muscle: transverse lattice elements (‘costameres’) mark sites of attachment between myofibrils and sarcolemma. *Proc. Natl. Acad. Sci.* **80**, 1008–1012 (1983).

26. Hoshijima, M. Mechanical stress-strain sensors embedded in cardiac cytoskeleton: Z

disk, titin, and associated structures. *Am. J. Physiol. Circ. Physiol.* **290**, H1313–H1325 (2006).

27. Bloch, R. J. *et al.* Costameres: repeating structures at the sarcolemma of skeletal muscle. *Clin. Orthop. Relat. Res.* **403**, S203--S210 (2002).

28. Samarel, A. M. Costameres, focal adhesions, and cardiomyocyte mechanotransduction. *Am. J. Physiol. Circ. Physiol.* **289**, H2291–H2301 (2005).

29. Ervasti, J. M. Costameres: the Achilles' heel of Herculean muscle. *J. Biol. Chem.* (2003).

30. A., S. M., Andrew, M. & K., B. T. Dance Band on the Titanic. *Circ. Res.* **91**, 888–898 (2002).

31. A., L. K., Rahul, K. & M., M. E. The Dystrophin Glycoprotein Complex. *Circ. Res.* **94**, 1023–1031 (2004).

32. Sabatelli, P., Pellegrini, C., Faldini, C. & Merlini, L. Cytoskeletal and extracellular matrix alterations in limb girdle muscular dystrophy 2I muscle fibers. *Neurol. India* **60**, 510–511 (2012).

33. Sharp, W. W., Simpson, D. G., Borg, T. K., Samarel, A. M. & Terracio, L. Mechanical forces regulate focal adhesion and costamere assembly in cardiac myocytes. *Am. J. Physiol. Circ. Physiol.* **273**, H546–H556 (1997).

34. Zemljic-Harpf, A., Manso, A. M. & Ross, R. S. Vinculin and Talin. *J. Investig. Med.* **57**, 849 LP-855 (2009).

35. Bray, M., Sheehy, S. P. & Parker, K. K. Sarcomere alignment is regulated by myocyte shape. *Cell Motil. Cytoskeleton* **65**, 641–651 (2008).

36. S., T. A., S., C. S., Wilson, N., K., H. S. & G., F. K. Focal Adhesion Kinase Is Activated and Mediates the Early Hypertrophic Response to Stretch in Cardiac Myocytes. *Circ. Res.* **93**, 140–147 (2003).

37. Komuro, I. Control of Cardiac Gene Expression by Mechanical Stress. *Annu. Rev. Physiol.* **55**, 55–75 (10AD).

38. Weiss, P. Shape and Movement of Mesenchyme Cells as Functions of the Physical Structure of the Medium: Contributions to a Quantitative Morphology. *Proc. Natl. Acad. Sci. - PNAS* **38**, 264–280 (3AD).

39. Gopalan, S. M. Anisotropic stretch-induced hypertrophy in neonatal ventricular myocytes micropatterned on deformable elastomers. *Biotechnol. Bioeng.* **81**, 578–587 (3AD).

40. Abrams, G. A., Goodman, S. L., Nealey, P. F., Franco, M. & Murphy, C. J. Nanoscale topography of the basement membrane underlying the corneal epithelium of the rhesus macaque. *Cell Tissue Res.* **299**, 39–46 (2000).

41. Goodman, S. L., Sims, P. A. & Albrecht, R. M. Three-dimensional extracellular matrix textured biomaterials. *Biomaterials* **17**, 2087–2095 (1996).

42. Pamuła, E., De Cupere, V., Dufrêne, Y. F. & Rouxhet, P. G. Nanoscale organization of adsorbed collagen: Influence of substrate hydrophobicity and adsorption time. *J. Colloid Interface Sci.* **271**, 80–91 (2004).

43. Wolf, K., Müller, R., Borgmann, S., Bröcker, E.-B. & Friedl, P. Amoeboid shape change and contact guidance: T-lymphocyte crawling through fibrillar collagen is independent of matrix remodeling by MMPs and other proteases. *Blood* **102**, 3262 LP-

3269 (2003).

44. Bettinger, C. J., Langer, R. & Borenstein, J. T. Engineering Substrate Topography at the Micro- and Nanoscale to Control Cell Function. *Angew. Chemie Int. Ed.* **48**, 5406–5415 (2009).

45. Curtis, A. S. G. & Wilkinson, C. D. W. Reactions of cells to topography. *J. Biomater. Sci. Polym. Ed.* **9**, 1313–1329 (1998).

46. Curtis, A. & Wilkinson, C. Topographical control of cells. *Biomaterials* **18**, 1573–1583 (1997).

47. Stevens, M. M. & George, J. H. Exploring and Engineering the Cell Surface Interface. *Science (80-.).* **310**, 1135 LP-1138 (2005).

48. Georges, P. C. & Janmey, P. A. Cell type-specific response to growth on soft materials. *J. Appl. Physiol.* **98**, 1547–1553 (2005).

49. E., I. D. Mechanical Signaling and the Cellular Response to Extracellular Matrix in Angiogenesis and Cardiovascular Physiology. *Circ. Res.* **91**, 877–887 (2002).

50. Wozniak, M. A. & Chen, C. S. Mechanotransduction in development: a growing role for contractility. *Nat. Rev. Mol. Cell Biol.* **10**, 34 (2009).

51. Suresh, S. Biomechanics and biophysics of cancer cells. *Acta Mater.* **55**, 3989–4014 (2007).

52. Curtis, A. S. G. *et al.* Substratum nanotopography and the adhesion of biological cells. Are symmetry or regularity of nanotopography important? *Biophys. Chem.* **94**, 275–283 (2001).

53. Berry, C. C., Campbell, G., Spadiccino, A., Robertson, M. & Curtis, A. S. G. The

influence of microscale topography on fibroblast attachment and motility. *Biomaterials* **25**, 5781–5788 (2004).

54. Bhattarai, S. R. *et al.* Novel biodegradable electrospun membrane: scaffold for tissue engineering. *Biomaterials* **25**, 2595–2602 (2004).

55. Abdul Kafi, M., El-Said, W. A., Kim, T.-H. & Choi, J.-W. Cell adhesion, spreading, and proliferation on surface functionalized with RGD nanopillar arrays. *Biomaterials* **33**, 731–739 (2012).

56. Gallagher, J. O., McGhee, K. F., Wilkinson, C. D. W. & Riehle, M. O. Interaction of animal cells with ordered nanotopography. *IEEE Trans. Nanobioscience* **99**, 24–28 (2002).

57. Biggs, M. J. P. *et al.* Interactions with nanoscale topography: Adhesion quantification and signal transduction in cells of osteogenic and multipotent lineage. *J. Biomed. Mater. Res. Part A* **91A**, 195–208 (2008).

58. Yang, P., Baker, R. M., Henderson, J. H. & Mather, P. T. In vitro wrinkle formation via shape memory dynamically aligns adherent cells. *Soft Matter* **9**, 4705--4714 (2013).

59. Bowden, N., Brittain, S., Evans, A. G., Hutchinson, J. W. & Whitesides, G. M. Spontaneous formation of ordered structures in thin films of metals supported on an elastomeric polymer. *Nature* **393**, 146 (1998).

60. Volynskii, A. L., Bazhenov, S., Lebedeva, O. V & Bakeev, N. F. Mechanical buckling instability of thin coatings deposited on soft polymer substrates. *J. Mater. Sci.* **35**, 547–554 (2000).

61. DuPont Jr., S. J., Cates, R. S., Stroot, P. G. & Toomey, R. Swelling-induced instabilities in microscale, surface-confined poly(N-isopropylacryamide) hydrogels. *Soft Matter* **6**, 3876–3882 (2010).

62. Au, H. T. H., Cheng, I., Chowdhury, M. F. & Radisic, M. Interactive effects of surface topography and pulsatile electrical field stimulation on orientation and elongation of fibroblasts and cardiomyocytes. *Biomaterials* **28**, 4277–4293 (2007).

63. Kim, D.-H. *et al.* Nanoscale cues regulate the structure and function of macroscopic cardiac tissue constructs. *Proc. Natl. Acad. Sci.* **107**, 565 LP-570 (2010).

64. McDevitt, T. C., Woodhouse, K. A., Hauschka, S. D., Murry, C. E. & Stayton, P. S. Spatially organized layers of cardiomyocytes on biodegradable polyurethane films for myocardial repair. *J. Biomed. Mater. Res. Part A* **66A**, 586–595 (2009).

65. Fu, C.-C. *et al.* Tunable Nanowrinkles on Shape Memory Polymer Sheets. *Adv. Mater.* **21**, 4472–4476 (2009).

66. Luna, J. I. *et al.* Multiscale Biomimetic Topography for the Alignment of Neonatal and Embryonic Stem Cell-Derived Heart Cells. *Tissue Eng. Part C Methods* **17**, 579–588 (2011).

67. Wang, P.-Y., Yu, J., Lin, J.-H. & Tsai, W.-B. Modulation of alignment, elongation and contraction of cardiomyocytes through a combination of nanotopography and rigidity of substrates. *Acta Biomater.* **7**, 3285–3293 (2011).

68. Liu, C., Qin, H. & Mather, P. T. Review of progress in shape-memory polymers. *J. Mater. Chem.* **17**, 1543–1558 (2007).

69. Meng, Q. & Hu, J. A review of shape memory polymer composites and blends.

Compos. Part A Appl. Sci. Manuf. **40**, 1661–1672 (2009).

70. Davis, K. A., Burke, K. A., Mather, P. T. & Henderson, J. H. Dynamic cell behavior on shape memory polymer substrates. *Biomaterials* **32**, 2285–2293 (2011).

71. Gall, K. *et al.* Thermomechanics of the shape memory effect in polymers for biomedical applications. *J. Biomed. Mater. Res. Part A* **73A**, 339–348 (2005).

72. McCain, M. L. & Parker, K. K. Mechanotransduction: the role of mechanical stress, myocyte shape, and cytoskeletal architecture on cardiac function. *Pflügers Arch. - Eur. J. Physiol.* **462**, 89 (2011).

73. Wang, Z. *et al.* Wrinkled, wavelength-tunable graphene-based surface topographies for directing cell alignment and morphology. *Carbon N. Y.* **97**, 14–24 (2016).

74. Hanft, L. M. Cardiac function and modulation of sarcomeric function by length. *Cardiovasc. Res.* **77**, 627–636 (12AD).

Vita

Shiyang Sun **ssun08@syr.edu**

Education

Syracuse University, Syracuse NY M.S. August 2016 to April 2019

Thesis Title "Dynamic change of Cardiomyocytes on Shape Memory Polymer"

Thesis Advisor: Dr. Zhen Ma

Jilin University, Jilin China B.S. September 2009 to July 2013

Posters Presentations

Sun S., Moore S., Wang C., Ash-Shakoor A., Henderson J., Ma Z. "*Dynamic Change of Human Stem Cell-Derived Cardiomyocytes on the Programmable Biomaterial Substrate"* Stevenson Biomaterials Lecture Series, Syracuse, NY 2019, *Poster*

Sun S., Moore S., Wang C., Ash-Shakoor A., Henderson J., Ma Z. "*Dynamic Change of Human Stem Cell-Derived Cardiomyocytes on the Programmable Biomaterial Substrate"* ECS Research Day, Syracuse, NY 2019, *Poster*

Sun S., Moore S., Wang C., Ash-Shakoor A., Henderson J., Ma Z. "*Dynamic Change of Human Stem Cell-Derived Cardiomyocytes on the Programmable Biomaterial Substrate"* CNY Cytoskeleton, Syracuse, NY 2019, *Poster*

Moore S., **Sun S.,** Wang C., Hoang P., Henderson J.H., Ma Z. "*Alignment of human cardiomyocytes through nano-wrinkles on shape memory polymers*" NEBEC, Rutgers, NJ 2019 *Oral*

Sun S., Moore S., Wang C., Ash-Shakoor A., Henderson J., Ma Z. "*Myofibril remodeling of human stem cell-derived cardiomyocytes responding to dynamic surface topography*" SFB, Seattle, WA 2019, *Rapid Fire*

Moore S., **Sun S.,** Wang C., Hoang P., Henderson J., Ma Z. "*Topographic alignment of human cardiac myocytes using shape memory polymers*" Summer UG Research Symposium, Syracuse, NY 2018 *Poster*